JOURNAL OF GEOPHYSICAL RESEARCH, VOL. 105, NO. B5, PAGES 10,939–10,960, MAY 10, 2000

Earthquake locations in southern California obtained using source-specific station terms

K. B. Richards-Dinger and P. M. Shearer

Institute of Geophysics and Planetary Physics, Scripps Institution of Oceanography
University of California, San Diego

Abstract. We relocate 297,400 events recorded by the Southern California Seismic Network (SCSN) between 1975 and 1998 using spatially varying station terms to improve relative location accuracy. Our method uses existing SCSN P and S picks, a smooth one-dimensional velocity model, and an iterative grid search approach based on the L1 norm. We apply empirical corrections for three-dimensional structure by computing station timing corrections that continuously vary as a function of source position. Station terms for each event are obtained by smoothing the residuals from nearby events using a natural neighbor (Delaunay) tessellation of the seismicity and then iterating until a stable set of locations and station terms is achieved. Our approach achieves relative location accuracy comparable locally to master event methods but can be applied uniformly over large regions. Median estimated standard errors for our final locations are 328 m in horizontal position and 741 m in depth. Our locations exhibit much less scatter, particularly in depth, than those of the SCSN catalog and a greater tendency to align into linear and planar features suggestive of fault structures. Our results appear comparable to, and in some cases better than, previous SCSN relocation studies using joint-hypocenter-velocity inversion techniques. Plots of daytime versus nighttime events permit discrimination between clusters of natural and artificial seismicity. We observe no simple relationship between the maximum depth of seismicity and surface geology.

1. Introduction

Earthquakes are routinely located by comparing observed arrival times of P and S phases with those predicted by a reference velocity model and by identifying the best fitting event locations and origin times. Inaccuracies in the assumed velocity model will introduce systematic errors into the locations; these errors are typically more significant than the mostly random errors caused by phase-timing uncertainties. For example, lateral velocity variations related to three-dimensional Earth structure will bias event locations derived using a one-dimensional velocity model. These errors can be divided into two different categories: (1) absolute location errors in individual events and (2) relative location errors among nearby events. Addressing the problem of absolute location errors requires solving for an improved velocity model; this is the approach used in joint-hypocenter-velocity (JHV) inversions [e.g., *Spencer and Gubbins*, 1980; *Pavlis and Booker*, 1980; *Hawley et al.*, 1981; *Thurber*, 1983; *Michael*, 1988; *Eberhart Phillips*, 1990; *Eberhart Phillips and Michael*, 1993; *Magistrale and Sanders*, 1996].

Paper number 2000JB900014.
0148-0227/00/2000JB900014$09.00

Improvements in relative locations among events, however, can be achieved without solving for a new velocity model. This has been accomplished using a variety of techniques, including joint epicenter determination, station term, and master event methods [e.g. *Douglas*, 1967; *Evernden*, 1969; *Lilwall and Douglas*, 1970; *Frohlich*, 1979; *Jordan and Sverdrup*, 1981; *Smith*, 1982; *Pavlis and Booker*, 1983; *Viret et al.*, 1984; *Pujol*, 1988]. These methods are most effective when applied to a relatively compact cluster of events, so that the travel time perturbation to each station is approximately constant among the different events. Of these approaches, perhaps the simplest and most widely applied is to solve iteratively for a custom set of station-timing corrections (commonly called "station terms"); this is the method described by *Frohlich* [1979].

For localized clusters of events these techniques often lead to a dramatic improvement in relative location accuracy (although the absolute location of the entire cluster remains poorly constrained). As the events become more distributed, however, these methods become less effective because a single set of station terms can no longer adequately describe the full effect of the three-dimensional velocity variations. For optimal results a different set of station terms is required for each source region. Researchers studying ways to improve earthquake locations have given these terms various names,

such as "source-specific site corrections" (SSSC), and "correction surfaces." If calibration events of known location are available, then improvements in absolute location accuracy can be achieved by suitable spatial interpolation of these terms [e.g., *Cogbill and Steck*, 1997; *Schultz et al.*, 1998].

Here we describe a new method for simultaneously locating large numbers of earthquakes that, on a local scale, achieves relative location accuracy comparable to master event techniques but which can be uniformly applied over a large area. Essentially, our approach is to compute station terms for each event by smoothing the residuals from nearby events using a natural neighbor (Delaunay) tessellation of the seismicity and then to iterate until a stable set of locations and station terms is achieved. Location errors are estimated using a bootstrap approach that randomly reassigns the final travel time residuals to different stations.

We apply our method to relocate nearly 300,000 earthquakes recorded by the Southern California Seismic Network (SCSN). Compared to the SCSN catalog, scatter in the event locations is substantially reduced, particularly in depth, and the earthquakes show a greater tendency to group into tight clusters and to align into linear and planar features.

2. Location Estimation

Any earthquake location method requires a measure of data misfit and a technique for identifying the minimum point in the misfit function.

2.1. Misfit Measures

The maximum likelihood estimates of source locations will be found by minimizing the appropriate norm (misfit function or measure) of the residuals, $r_{ij}(t_i, \vec{x}_i) \equiv T_{ij}^{\text{obs}} - t_i - \tau_j(\vec{x}_i)$ (where t_i and $\vec{x}_i$ are the origin time and location of the ith event respectively, T_{ij}^{obs} is the observed arrival time at the jth station from the ith event, and $\tau_j(\vec{x})$ gives the travel time to the jth station from a source at $\vec{x}$) with respect to the origin times and source locations (see Appendix A for discussion). Thus one must know seismic velocity as a function of position (to calculate the $\tau_j(\vec{x})$) and the distribution of the picking errors (which determines the misfit function). We will defer discussion of the velocity model to section 2.3, and we now discuss the choice of misfit function. It is common practice, at least for routine processing, to use the L2 norm, that is, to minimize the weighted sum of the squares of the residuals. As discussed in Appendix A, this least squares misfit function is appropriate for independent zero-mean normally distributed errors. However, distributions of travel time residuals are rarely Gaussian, usually having much longer tails than Gaussian distributions [e.g., *Jeffreys*, 1932; *Buland*, 1984; *Freedman*, 1966; *Pulliam et al.*, 1993; *Billings et al.*, 1994]. While least squares gives the maximum likelihood estimate (and therefore is asymptotically fully efficient in the statistical sense of having the minimum variance [*Kendall and Stuart*, 1967]) for errors which are normally distributed, it is not robust with respect to deviations from the normal distribution. Even if only a small fraction of the errors are drawn from a distribution with longer than Gaussian tails (or from another Gaussian distribution broader than the main one), least squares estimates are less efficient than other more robust estimates [e.g. *Huber*, 1981].

For this reason, we use the L1 norm for our relocation algorithm; that is, we minimize the sum of the absolute values of the residuals. This approach yields the maximum likelihood estimators if the distribution of errors is double-sided exponential, pays only a small efficiency penalty if the distribution is actually Gaussian, and, most relevantly, is more efficient than the L2 norm for distributions with tails heavier than Gaussian [*Huber*, 1981]. The L1 norm is simpler to implement than many other robust misfit measures (e.g., bisquare, Huber, sine, Jeffreys [see *Anderson*, 1982]) because it requires no tuning of parameters and, like least squares, is well-suited for efficient computation of origin times and station corrections.

2.2. Minimization Techniques

There are a variety of methods to identify the minimum in the event location misfit function. The traditional way, apparently dating back to at least *Geiger* [1910], is to use least squares and to expand the residuals in a first-order Taylor series about some initial guess for t_i and $\vec{x}_i$. The resulting linear least squares problem is then solved via the normal equations (or modifications thereof; [see *Thurber*, 1986, and references therein]) to yield an improved location estimate, and the method then iterates to convergence. Other misfit criteria can be handled using a similar approach by iteratively reweighting the residuals to simulate the desired misfit measure [*Anderson*, 1982]. All of these methods require calculation of partial derivatives of τ_j. In addition, the normal equations can suffer from stability problems, depending on the condition number of the matrix of partial derivatives (though the modifications mentioned above alleviate this problem to some extent). More recently, various nonlinear minimization schemes, which do not require derivative information and do not suffer the same stability problems, have been applied to the earthquake location problem, including grid search methods [*Sambridge and Kennett*, 1986; *Nelson and Vidale*, 1990], genetic algorithms [*Sambridge and Gallagher*, 1993], simulated annealing [*Billings et al.*, 1994], and evolutionary programming [*Minster et al.*, 1995]. We use a grid search approach similar to that of *Sambridge and Kennett* [1986] and *Shearer* [1997], which we will describe in more detail in section 5.

2.3. Velocity Model Errors

In addition to the random errors ϵ_{ij} resulting from picking arrival times from (noisy) seismograms, there

are also systematic errors caused by the difference between the actual seismic velocity structure and the one used to calculate the predicted travel times. These errors will bias the estimated locations away from the true locations. For events recorded and picked using exactly the same set of stations (i.e., identical numbers of P and S picks from identical stations) this bias will vary as a function of source location but will be similar for "nearby" events (where the definition of nearby will depend mostly on the scale length of the unmodeled structure) so that the relative locations of nearby events will be preserved. Unfortunately, for the SCSN catalog at least, even nearby events are recorded by widely varying subsets of the entire network. For example, of the 16,187 events in our catalog in a square box 50 km on a side surrounding the 1994 Northridge mainshock, 16,117 were recorded by unique subsets of the SCSN network; that is, they have a unique set of P and S picks matched by no other event. Of the remaining events, there were 29 pairs of events recorded by the same subnetwork, no triplets and three quadruplets. This interaction of the variation of effective network geometry with velocity model errors leads to psuedo-random scatter in the estimated locations [e.g., *Pavlis and Hokanson*, 1985]. Depending on accuracy of the velocity model used to calculate the travel times τ_j, this psuedo-random scatter may dominate the truly random scatter from the random reading errors ϵ_{ij}. Some of these biasing effects could be reduced by using a subset of the data with a more consistent network geometry but at the cost of discarding part of the available data. A more efficient approach is to use station terms to adjust for differences in the travel times to the different stations.

3. Static Station Terms

A first step toward accommodating (and therefore removing the bias caused by) unmodeled structure is the use of station corrections or station terms. When locations are estimated as above for a number of events, it is often found that the distributions of residuals at individual stations have nonzero means and are much more compact than the distribution of all residuals taken together. This indicates that a significant part of the modeling error at each individual station is common for all events. This part of the modeling error can be accounted for by the use of a single number at each station (actually a single number for each phase) which is added to the $\tau_j(\vec{x})$ calculated from the velocity model. Thus we obtain a new version of equation (A1):

$$T_{ij}^{\text{obs}} = t_i + \tau_j(\vec{x_i}) + s_j + \epsilon_{ij}, \qquad (1)$$

where s_j is the station correction or station term for the jth station. We will refer to these as static station terms to differentiate them from the source-specific station terms discussed in section 4. Notice that now the (L1) misfit function to be minimized is a function of the s_j in addition to the t_i and the $\vec{x_i}$:

$$C_s(t_i, \vec{x_i}, s_j) = \sum_{i,j} w_{ij} \left| T_{ij}^{\text{obs}} - t_i - \tau_j(\vec{x_i}) - s_j \right|. \qquad (2)$$

We note here that because analyst estimates of picking error are only available for about half of the data in the SCSN catalog, for this data set we actually set all of the weights w_{ij} to 1.0; see Appendix A for more discussion. Taking derivatives of C_s with respect to t_i, $\vec{x_i}$, and s_j will give $4n_q + n_s$ equations for the $4n_q$ unknown hypocentral parameters and the n_s unknown station corrections. This system (unlike the set of equations without station corrections; see Appendix A) does not decouple: the derivatives with respect to the hypocentral parameters of any event will involve the station corrections for any stations that recorded that event, and the derivatives with respect to a station correction will involve the hypocentral parameters of any event that was recorded by that station.

We perform the minimization of C_s with a two-step iterative procedure based on that of *Frohlich* [1979]. In the first step the station corrections s_j are held fixed and C_s is minimized with respect to the hypocentral parameters. In this step we simply absorb the station corrections into the arrival times to form "corrected" arrival times, $T_{ij}^{'\text{obs}} \equiv T_{ij}^{\text{obs}} - s_j$ and locate each event as before but with these corrected arrival times instead of the actual arrival times. In the second step the hypocentral parameters are held fixed and C_s is minimized with respect to the station corrections. In this step, from equation (2), each s_j is just given by the weighted median (see Appendix B) of the residuals at that station, $T_{ij}^{\text{obs}} - t_i - \tau_j(\vec{x_i})$. In the case of the L2 norm a similar method can be applied, using the weighted mean instead of the median. We repeat these two steps until they converge to a stable set of station corrections and hypocentral parameters. There is one very fundamental nonuniqueness in equation (2); if we add some δt to all the origin times t_i and subtract the same δt from all the station terms s_j, the value of the misfit function is unchanged. We resolve this in the usual way of constraining the mean of the station terms to be zero.

4. Source-Specific Station Terms

Station corrections as described in section 3 work well only when the differences between the actual travel times in the Earth and those in the assumed velocity model to each station are the same for all events. The two most relevant situations where this would occur are when (1) errors in the assumed velocity model are confined to very shallow depths and (2) the events are confined to a region small compared to the event-station separations and dominant scale length of the errors in the assumed velocity model. In the latter case the use of station terms is similar to using master event relocation methods, where the relative locations of the events with respect to each other are much better determined than

the absolute location of the cluster as a whole [e.g., *Jordan and Sverdrup*, 1981]. When the seismicity covers a large region containing significant lateral velocity heterogeneity, neither of the above two conditions is likely to apply. One approach to dealing with this problem is to jointly invert for event locations and perturbations to the assumed velocity model [e.g., *Spencer and Gubbins*, 1980; *Pavlis and Booker*, 1980; *Hawley et al.*, 1981; *Thurber*, 1983; *Michael*, 1988; *Eberhart Phillips*, 1990]. However, it is possible to improve the relative locations of nearby events (even in the presence of three-dimensional velocity heterogeneity) without inverting for a velocity model by generalizing the station term concept. In this case, the station corrections no longer consist of a single term at each station; rather, each station will have a station correction function which will vary as a function of source position.

This concept is related to observations of azimuthally varying station terms [e.g., *Cleary and Hales*, 1966; *Herrin and Taggart*, 1968; *Lilwall and Douglas*, 1970; *Dziewonski and Anderson*, 1983]. More recently, this idea has been extended to include takeoff angle as well as azimuth [e.g., *Zhou and Wang*, 1994; *Robertson and Woodhouse*, 1997]. For purposes of earthquake location, however, perhaps a more straightforward approach is to parameterize the station terms directly in terms of event location, as first suggested by *Pavlis and Hokanson* [1985]. A simple way to implement this (used, for example, by *Seeber and Armbruster* [1995]) is to define a set of boxes and to calculate a separate set of static station corrections for each box. Disadvantages to this approach include uneven event density and the discontinuous changes in the station correction functions at the boundaries of the boxes. Other more elaborate methods of defining these station correction functions are given by *Cogbill and Steck* [1997] and *Schultz et al.* [1998]. In general, these studies have considered only two-dimensional variations in the station corrections, although in principle, they could be generalized to include variations with event depth.

We use a different approach which is essentially a generalization of that of *Frohlich* [1979] for estimating a set of static station corrections. It remains a two-step iterative process, but now the station correction estimation step is more elaborate. For static station terms we simply calculate the station term for each station as the weighted median of the residuals at that station from all events. For source-specific station terms (SSSTs), we calculate a separate correction for each source-receiver pair as the weighted median of the residuals at the given station from N nearby events. If N is equal to the total number of events, we recover the static station term case. If we set N equal to 1, then we have the meaningless case of every SSST being completely independent of the others, and we will obtain a misfit of zero with the events remaining at any arbitrary initial set of event locations. For intermediate values of N we will obtain station correction functions which vary smoothly as a function of source location (in both position and depth), with the degree of smoothing determined by the choice of N. The SSSTs so computed will adapt naturally to event density, averaging over larger volumes where seismicity is sparse and over smaller volumes in regions of dense seismicity.

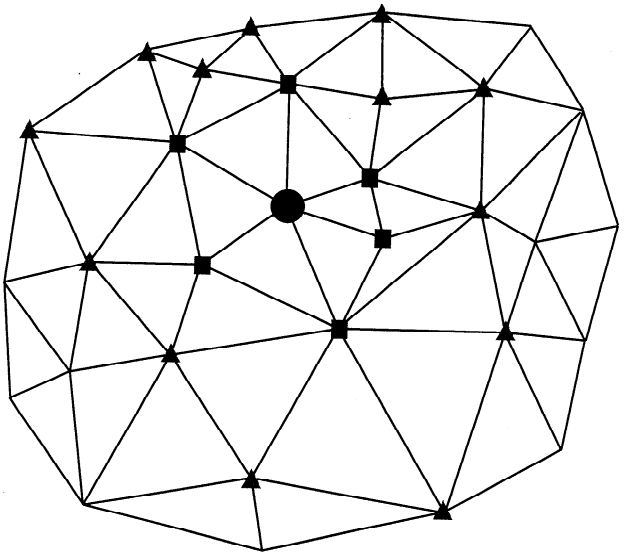

Figure 1. An example of a 2-D Delaunay tessellation of a set of 31 points. If the point denoted by a circle is the event under consideration, then the squares mark its first-order natural neighbors and the triangles mark its second-order natural neighbors.

A key feature of our method is the way in which we determine the N adjacent events to each target event. We select nearby events using the concept of Delaunay tessellation and natural neighbors, methods widely used in computational geometry, but only recently introduced to geophysics [e.g., *Parker et al.*, 1987; *Hildebrand and Parker*, 1987; *Constable et al.*, 1993; *Sambridge et al.*, 1995; *Braun and Sambridge*, 1995]. For a given set of points in three dimensions the Delaunay tessellation specifies connections between a given set of irregularly distributed points, or nodes, that define tetrahedra that are as "well-shaped" as possible. The "natural neighbors" of each point are those points that are directly connected by the Delaunay tessellation; they are the closest surrounding points and are uniquely defined by the nodal distribution. Here we generalize this concept, defining a pair of points to be ith-order natural neighbors if i is the minimum number of edges of the Delaunay tessellation which must be traversed to travel from one point to the other.

The number of ith order natural neighbors is not fixed but will vary from node to node depending upon the geometry of the tessellation. To choose the N nearest natural neighbors of an event, we construct (using the code of *Barber et al.* [1996]) the 3-D Delaunay tessellation of the current locations and select the N lowest-order natural neighboring events, taking a random sample of the

last order if necessary to get exactly N events. In the (two-dimensional) example shown in Figure 1, the circle is the target event, the squares are its first-order natural neighbors, and the triangles its second-order natural neighbors. For the 15 nearest natural neighbors we would use all six first-order and a randomly selected nine of the 13 second-order natural neighbors. Depending upon the density of the events surrounding the target event, the nearest neighbors can span a wide range of distances. The Delaunay tessellation ensures that the computed SSSTs vary smoothly and continuously throughout the event distribution.

5. Data and Processing

Southern California provides a good test of our relocation algorithm. Over 300,000 local events have been recorded since 1975 and are widely distributed across the region. The area has been well-studied, and phase data from a large network are readily available.

5.1. Data

Our data are the arrival times of P and S waves from 297,400 local events from 1975, 1976, and 1981-1998 recorded at the more than 200 stations of the Southern California Seismic Network (SCSN) [e.g., *Wald et al.*, 1995], a joint project of the Seismological Laboratory, California Institute of Technology, and the U.S. Geological Survey, Pasadena. Figure 2a shows the locations of the SCSN stations. These arrival times are manually picked by SCSN analysts and are available from the Southern California Earthquake Center Data Center (SCECDC) (http://www.scecdc.scec.org). The arrivals are used by the SCSN to locate the events (using an iterative least squares approach), producing an event catalog (hereinafter referred to as the SCSN catalog). We use these results as starting locations for our relocation scheme. To avoid P_g/P_n and S_g/S_n ambiguity, we use only arrivals with source-receiver ranges of 120 km or less. We relocate only those events with at least five such picks. Our final data set contains 4,147,998 P and 846,350 S arrivals.

5.2. Grid Search Algorithm

To identify the best fitting location for each event, we use the grid search algorithm described by *Shearer* [1997], which is similar to that of *Sambridge and Kennett* [1986]. For each event we calculate the misfit at each point in a precomputed grid (see section 5.3) in a region which covers the entire depth extent of the grid and is 20 km × 20 km laterally, centered on the SCSN catalog epicenter. Note that a grid search for the origin time is unnecessary; for the L1 norm and equation (2) and a given $\vec{x_i}$, the t_i which minimizes C_i is simply given by the weighted median (see Appendix B) of the $T_{ij}^{'\text{obs}} - \tau_j(\vec{x_i})$, where the $T_{ij}^{'\text{obs}}$ are the corrected arrival times. In the case of the L2 norm a similar argument

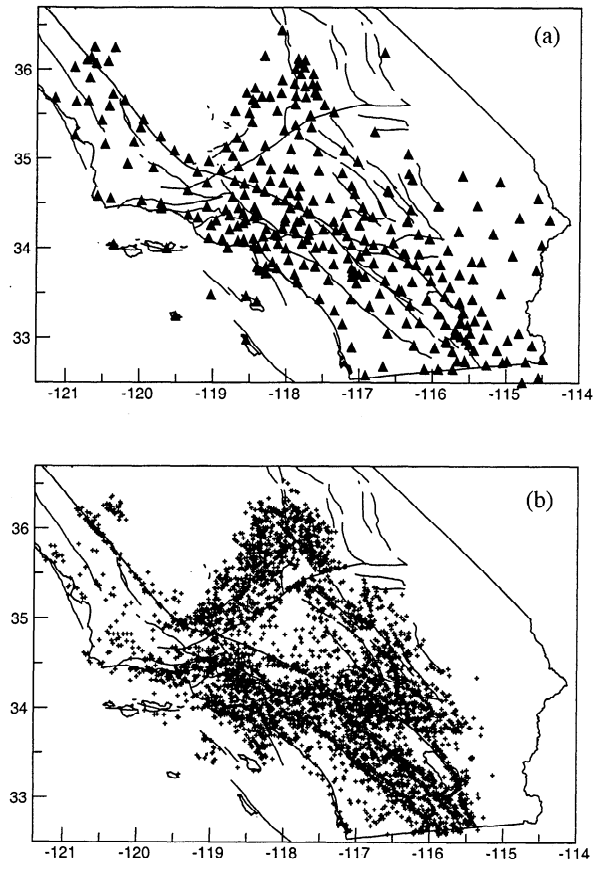

Figure 2. (a) Locations of SCSN stations within our study area. Heavy lines are state boundaries and coastlines; light lines are faults. (b) Locations of the 5226 sources used to calculate our static station terms.

applies and the best fitting origin time is obtained from the weighted mean.

Following identification of the best fitting grid point, we refine the search by finding the misfit for each point in a series of successively finer 3 × 3 × 3 grids centered on the best fitting point from the previous grid search. The spacing in the final grid is ~15 m; this is the nominal resolution of our method. The travel times from the points in these finer grids are obtained by interpolation from the surrounding points in the precomputed grid. If the best fitting point is at the edge of the initial search grid, indicating that the minimum may lie outside the initial search grid, the search is restarted with a new, shifted, initial search grid.

5.3. Precomputation of Travel Times

For a reference 1-D velocity model we use a smoothed version [*Shearer*, 1997] of the standard southern California velocity model [*Wald et al.*, 1995; *Hadley and Kanamori*, 1977]. We assume a scaled version of the P velocity model for the S velocity model, using a Poisson's ration of 0.25. From these models we compute P and S travel time tables at 2-km intervals of range and

source depth. To speed the evaluation of travel times from trial locations to the SCSN stations, we then precompute and store the travel times from a grid covering southern California to each of the SCSN stations by interpolating from these travel time tables. The grid covers latitudes from 32.5°N to 36.7°N, longitudes from 121.4°W to 115°W, and depths from 0 to 26 km, with a spacing of ~2 km. The spacing between grid points must be small enough to insure adequate sampling of the travel time curves. We interpolate travel times between these grid points using trilinear (in early iterations) and tricubic (in later iterations) interpolation. The trilinear interpolation is much faster to compute but results in slight second-order discontinuities (i.e., changes in slope) in the travel times at the grid points. In some cases this can produce artifacts in the locations with some events tending to "stick" near the grid points. These artifacts are eliminated through use of the tricubic interpolation, which yields smooth variations in travel time with position.

5.4. Test of Grid Search Algorithm

To test how well our grid search algorithm works, including the effects of its various interpolations, we perform a simple synthetic test. For each event in the SCSN catalog we generate synthetic arrival times for each station which recorded that event by ray tracing from the catalog location through our 1-D reference velocity model. These times are generated by solving the two-point ray tracing problem exactly; we avoid using travel time tables at this stage. We then apply our algorithm to locate the events using the synthetic arrival times. Since there is no added noise, each event should be located at its catalog location (to within the resolution of our finest grid). Any differences are errors introduced by inaccuracies in the various interpolations and/or the failure of our grid search algorithm to find the minimum in the misfit function. For the 297,400 catalog events, the median difference between the initial and recovered locations is 9.7 m in horizontal position and 42.7 m in depth. These differences are much less than the typical standard errors in the event locations derived from the actual data (see section 5.7), implying that the small errors introduced by the travel time interpolations do not limit the accuracy of our locations.

5.5. Static Station Terms

To account for shallow velocity differences below each station, we first estimate static station terms using a set of 5226 well-recorded events distributed as evenly as possible across southern California (see Figure 2b). We select these events by dividing our study volume into boxes with dimensions approximately 7 km × 7 km × 4 km. From each box we choose the event with the largest number of picks from those which have an SCSN catalog location quality of "A" or "B" and which have at least one S pick within 25 km of the epicenter. We do not use the complete catalog at this stage to avoid the biasing influence of large numbers of events in certain areas (e.g., Landers, Northridge). Figure 3 shows our computed P and S static station terms as a function of station location. The P static station corrections vary from about −0.6 to 0.6 s and the S vary from −0.8 to 1.5 s. The most obvious features in these maps are the large positive station corrections associated with the slow near-surface velocities in the sedimentary basins, including Ventura, Los Angeles, and the Salton Trough. The P and S station corrections are highly correlated with the S terms ~2.3 times larger than the P terms.

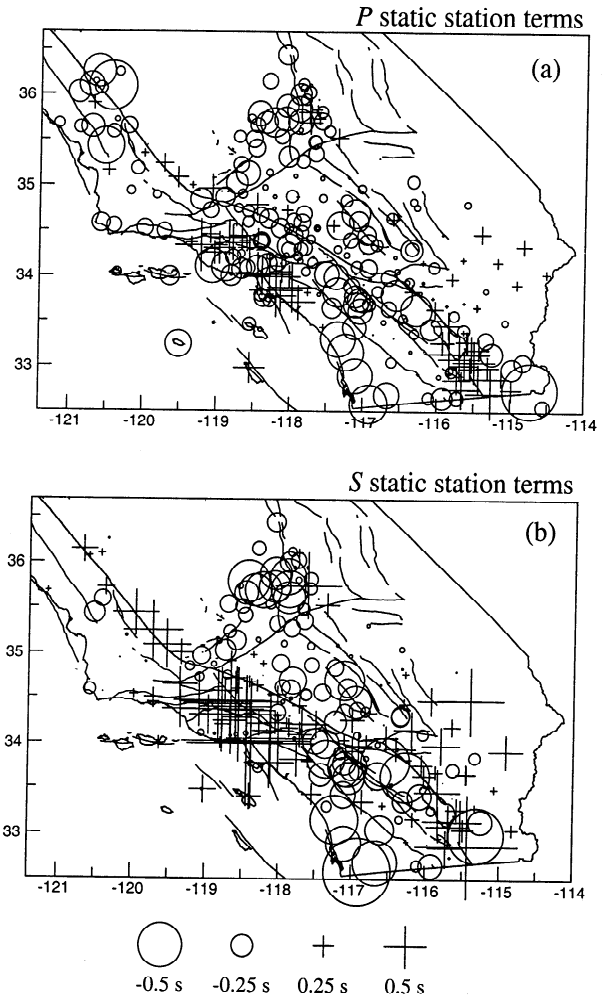

Figure 3. (a) Our P static station terms plotted at the station locations, with circles denoting negative (early) station terms and crosses indicating positive (late) station terms. Note the large positive station corrections in the major sedimentary basins (Ventura, Los Angeles, and Salton Trough) and generally negative station corrections elsewhere. (b) Same as Figure 3a, except for S station terms.

5.6. Source-Specific Station Terms

Our basic algorithm is quite simple and can be described by the following steps:

1. Locate all events using the previously determined static station terms.

2. Construct the 3-D Delaunay tessellation of the current locations.

3. For each source-receiver pair (for which a pick exists) calculate a source specific station term (SSST) as the median of the residuals from the N nearest natural neighbor events which have picks at the station in question.

4. Relocate the events using these SSSTs.

5. Iterate steps 2, 3, and 4 until some measure of convergence is satisfied.

Although this basic algorithm worked well in most regions, we identified artifacts in our computed locations in some areas where the one-dimensional velocity model was particularly inappropriate. One example occurred in the Salton Trough for seismicity along the Imperial Fault. Some clusters of events, which in fact all occurred at roughly the same depth, would separate upon initial location into two clusters at different depths, one cluster containing those events for which an S arrival had been recorded at a nearby station and the other cluster containing those events without a nearby S pick. In some cases these clusters were separated enough that the subsequent iterations would not reconcile the depths, and the clusters would remain separate.

This problem could have been avoided by locating events only in those regions where the velocity model was reasonably accurate or by restricting analysis to only those events with nearby S picks. However, our goal was to develop a method that could be applied to relocate the complete SCSN catalog, so we modified our basic algorithm to avoid these artifacts by first locating those events which have at least one S pick within 25 km of the epicenter and then adding in the other events in subsequent steps. The full algorithm is given in Appendix C.

The convergence of the algorithm may be evaluated (Figure 4) in terms of both the scaled median absolute deviation (SMAD, a robust measure of the spread of a distribution which is equal to the standard deviation for Gaussian distributions) of the residuals and the median change in location from one iteration to the next. The non-S events (see Appendix C) were added in at iteration 6, explaining the blips at that iteration in the otherwise monotonic curves.

The choice of N, the number of nearest neighbors over which we average the residuals to obtain the SSSTs, is subject to the usual trade-off between resolution and accuracy. A larger N should provide better cancellation of the random errors, at the cost of averaging a spatially varying quantity over a larger volume. On the basis of experiments on subsets of the catalog with several different values of N, we select $N = 50$ as a reasonable compromise. This leads to averaging volumes with dimensions as small as a few hundred meters in areas of dense seismicity and as large as a few hundred kilometers horizontally and the full depth extent of the model

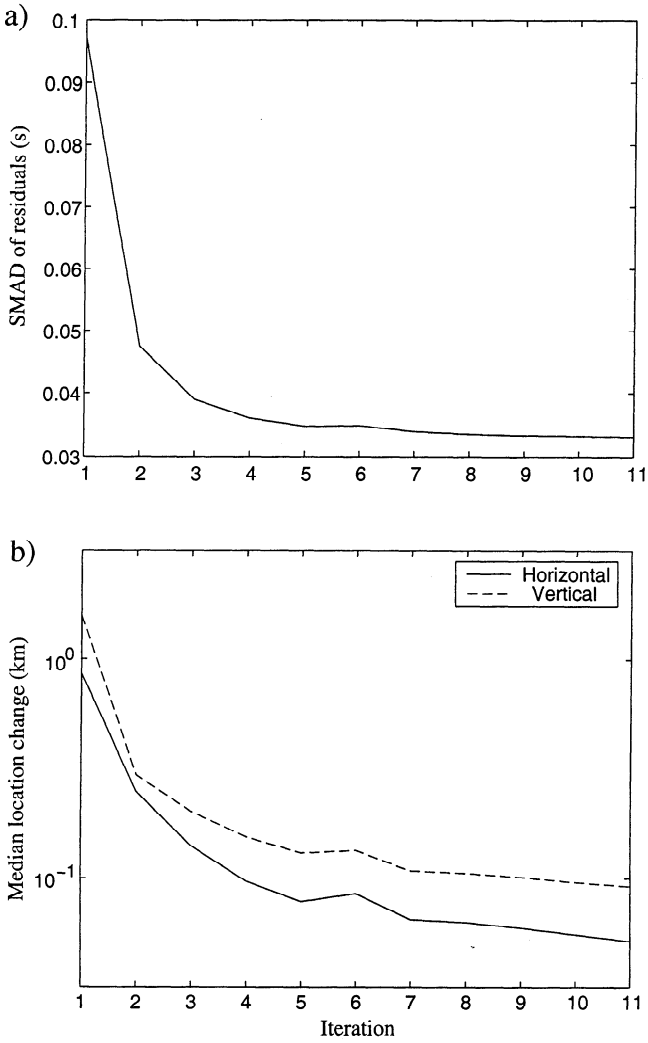

Figure 4. (a) The SMAD of the residuals (P and S together) at each iteration. (b) Median of the difference in the locations of the events at each iteration relative to each event's location at the previous iteration. The first five iterations used only events with nearby S picks, while subsequent iterations included all events, explaining the blips at iteration 6 in the otherwise monotonically decreasing curves.

vertically in areas of sparse seismicity. Typically, the averaging volumes have dimensions of a few kilometers. Because we treat the P and S SSSTs completely separately, the averaging volume for S is generally somewhat larger than that for P, owing to the smaller number of S picks.

We show an example of our SSSTs for one particular station in Figure 5. In Figure 5a we plot the P residuals for every event recorded at station RYS at each event's location projected to the surface. The static station correction for RYS has already been applied, so the median residual is zero. Note the spatial coherence of the pattern of residuals, indicative of the presence of 3-D velocity heterogeneity. Figure 5b is a similar plot of our P SSSTs for RYS calculated from the residuals

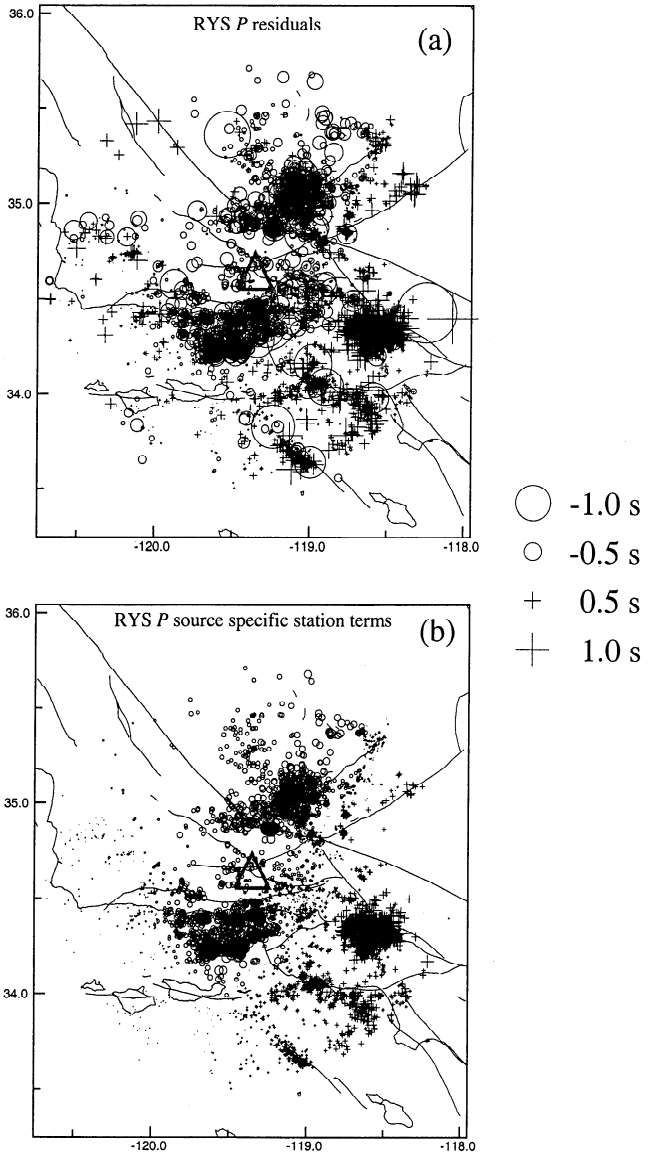

Figure 5. (a) P residuals for all events recorded by station RYS (large triangle) plotted at the event locations. The static station correction has already been applied. Note the large-scale spatial coherence in the residual pattern, indicating the presence of 3-D velocity heterogeneity. (b) The source-specific station terms (SSSTs) for station RYS calculated from the residuals in Figure 5a, again plotted at the event locations. The number of nearest natural neighbors, N, is 50. The SSSTs are essentially a spatially smoothed version of the residuals.

in Figure 5a. Note that the SSSTs are essentially a spatially smoothed version of the residuals. For all events the S SSSTs are positively correlated with the P SSSTs with a correlation coefficient of 0.75, and the slope of the line which best fits (in an L1 norm sense) a plot of S SSSTs versus P SSSTs is 2.5.

5.7. Location Uncertainty Estimation

We estimate location errors using the random resampling approach of *Billings et al.* [1994] as modified by *Shearer* [1997]. We assume that the distribution of the final travel time residuals ($T_{ij}^{\rm obs} - t_i - \tau_j(\vec{x}_i) - s_{ij}$, where the s_{ij} are the SSSTs) from a given final location is representative of the distribution of random timing errors for that event. We simulate the effect of these errors on the computed location by randomly selecting residuals (from the complete set of residuals for the event) to add to each arrival time and then relocating the event using these perturbed arrival times. By repeating this procedure many times, we obtain a cloud of possible locations for the event that represents the scatter due to the uncertainties in the picks. This technique has the advantages of fully including all of the nonlinearities of the problem and the fact that some ray paths are much more important than others in constraining the location. The median horizontal standard error for the entire catalog is 328 m, and the vertical is 741 m. Note that since we hold the SSSTs fixed during this procedure, these error estimates are a measure of the relative location errors among nearby events produced by random errors in the arrival times. They do not include the systematic errors in absolute event location introduced by incorrect velocity models and/or three-dimensional velocity heterogeneity. The improvement in location accuracy achieved by applying the SSSTs is primarily in the relative locations among nearby events.

Evaluating absolute location accuracy is hindered by the fact that the true locations of the vast majority of events are unknown. In principle, a subset of events of known locations would provide a good test of our location procedure. Ideally, these events would be distributed similarly to the entire catalog so that (1) the distribution of errors of these events would be representative of that of the complete catalog, (2) we could test how the error varies as a function of event position, event magnitude, number of picks, etc., and (3) closely spaced events could be used to check relative location error, as well as absolute location errors. In addition, these known locations could be incorporated into the location procedure as constraints (by increasing the weights, w_{ij} in equation (2), associated with the phases from these events), improving the absolute locations. Unfortunately, the only events whose location we can truly know are explosions. These are nonideal as they are confined to the surface (whereas natural seismicity occurs at depth) and thus their travel times include the effects of traversing the often highly heterogeneous near-surface region twice. In addition, their geographical distribution is also quite different from natural seismicity. Nonetheless, we compared the known locations of 58 such events [*Hauksson*, 2000] with the locations for the same events in the SCSN catalog and in our final catalog. In both cases, the median horizontal mislocation was ~750 m.

5.8. Residuals

Histograms of the P and S residuals for the catalog locations, our locations with static station terms,

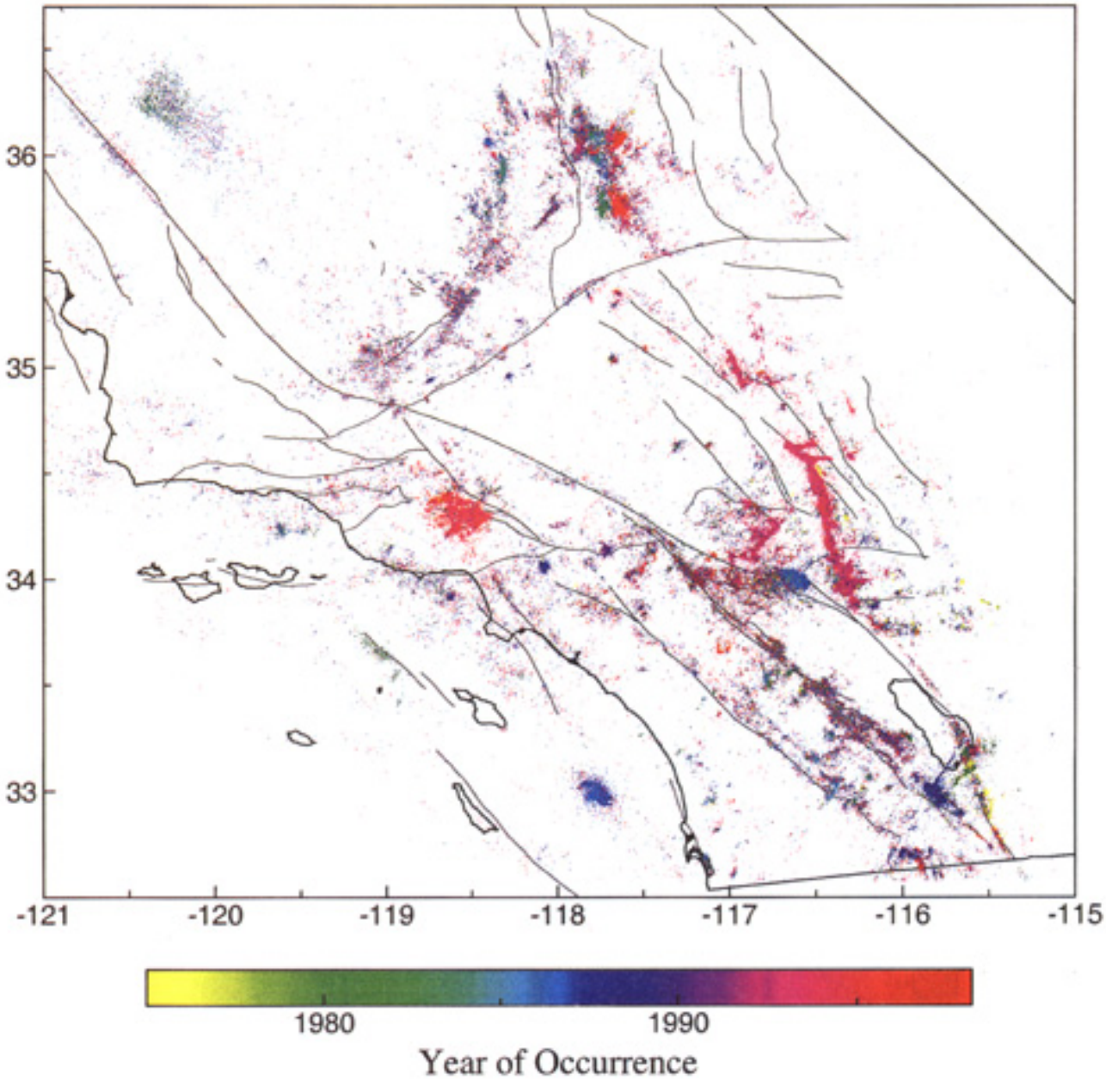

Plate 1. A map view of our final relocations. The events are colored by the date of their occurrence, so that temporally limited clusters appear coherent, whereas areas of ongoing seismicity appear multicolored.

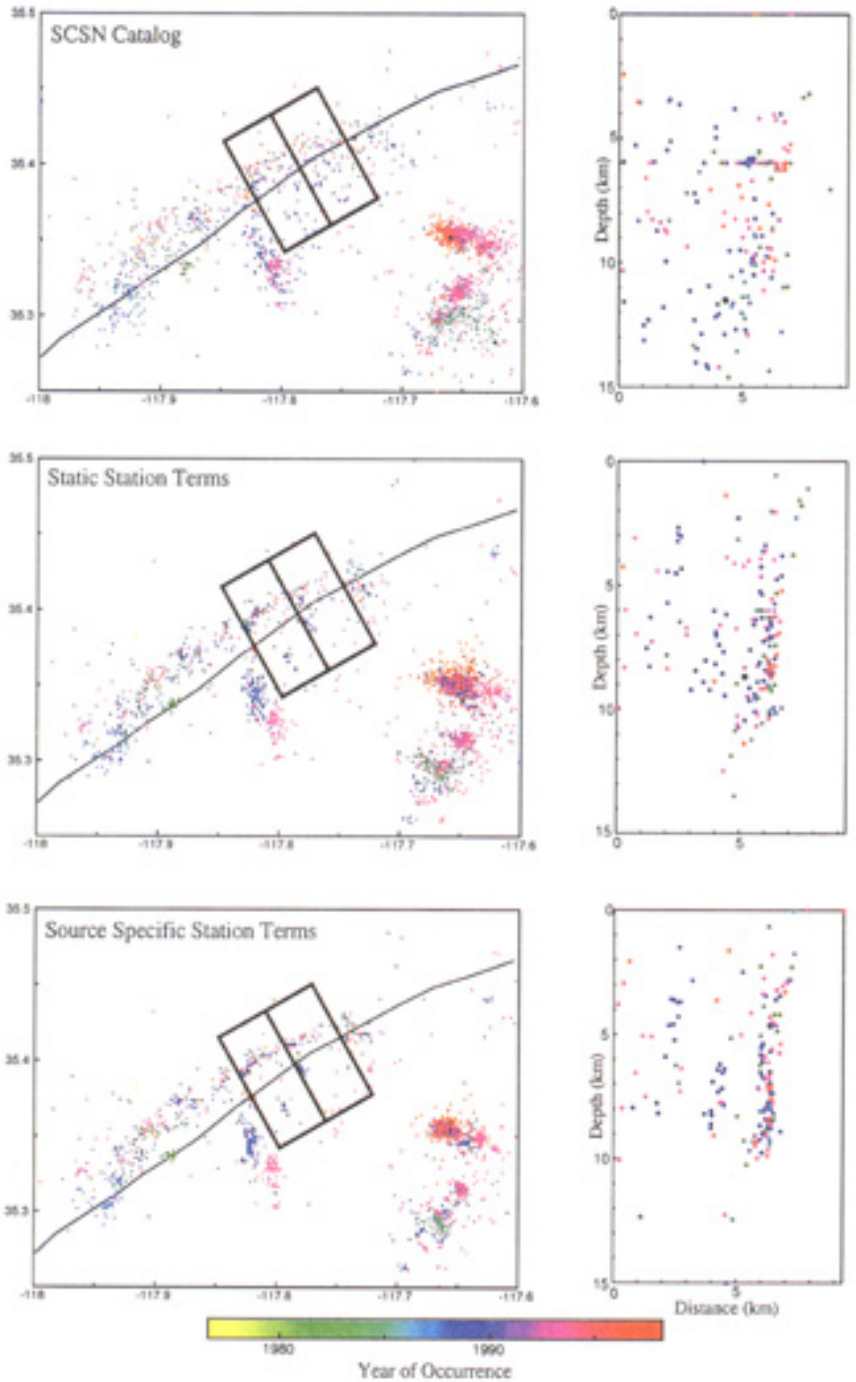

Plate 2. (left) Map views and (right) SSE-NNW cross sections of (top) the SCSN catalog locations, (middle) our static station term relocations, and (bottom) our source-specific station term relocations of seismicity on and near the Garlock fault.

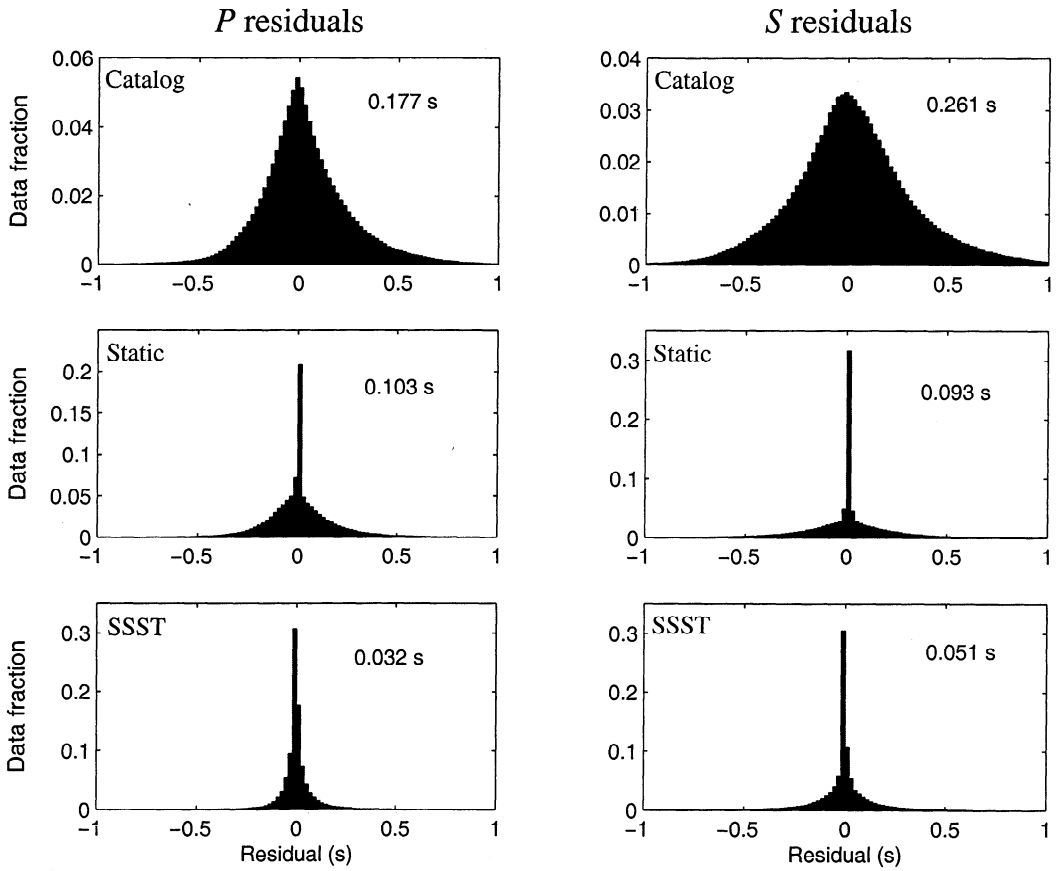

Figure 6. Residual histograms. (top) SCSN catalog residuals, (middle) residuals from locations using our static station terms, (bottom) residuals from our final locations using our SSSTs. (left) P residual histograms and (right) S residual histograms. The SMAD of each distribution is indicated on each plot.

and our locations with SSSTs are presented in Figure 6. The distributions of the residuals for the latter two sets of locations show the sharp peaks at zero typically seen with the use of the L1 norm. On each plot we indicate the SMAD of each distribution. For the P residuals, the SMADs decrease from 0.177 s to 0.103 s to 0.032 s for the three sets of locations, respectively. Similarly, the SMADs of the S residual distributions decrease from 0.261 s to 0.093 s to 0.051 s. Squaring the SMADs to get a robust version of variance gives a "variance" reduction of 66% for P and 87% for S with the addition of the static station terms. The addition of the SSSTs further improves the variance reduction to 97% for P and 96% for S.

Of course, some improvement in model fit should be expected when more free parameters are permitted in an inversion. However, the use of static station terms and SSSTs leads to a large improvement in the model fit while adding only a relatively small number of additional free parameters. We are locating about 300,000 events using about 5 million arrival times. There are four model parameters associated with each location and one model parameter for each station associated with the static station terms. A reasonable estimate for the number of effective model parameters associated with the SSSTs is the number of picks divided by N (which is 50 in our case). Thus, since the number of events is about 300,000 and the total number of picks is about 5 million, the total number of model parameters used in the three sets of locations are approximately 1.2 million, 1.2 million, and 1.3 million for the catalog, static station term, and SSST locations, respectively.

6. Relocation Results

Our final catalog consists of locations and estimated standard errors for 297,400 events (available via anonymous ftp at ftp://mahi.ucsd.edu/pub/SSST). Events may be identified by their times and their SCSN CUSP number. We now describe some of the main features of the locations and compare our results to those of the SCSN catalog and some other relocation results. These include the locations of *Zhou* [1994], *Seeber and Armbruster* [1995], *Magistrale* [1993], *Magistrale and Sanders* [1996], and *Hauksson* [2000].

6.1. Overview

We plot a map view of all our final locations in Plate 1. Each event is colored by the date of its occurrence, and areas of ongoing seismicity are multicolored,

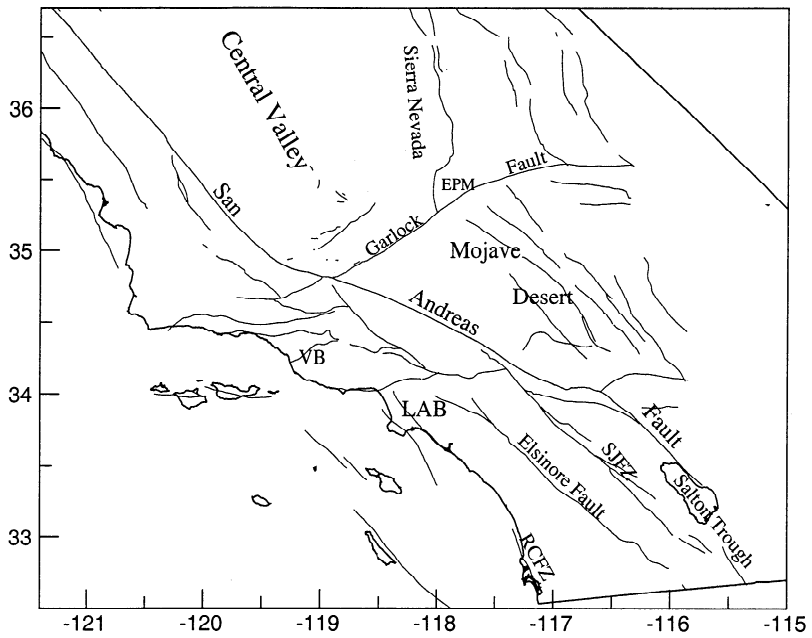

Figure 7. Map labeling faults and geographic features mentioned in the text. Abbreviations are El Paso Mountains (EPM), Ventura Basin (VB), Los Angeles Basin (LAB), San Jacinto Fault Zone (SJFZ), and Rose Canyon fault zone (RCFZ).

whereas temporal clusters of seismicity, such as large events and their aftershocks, appear as coherently colored regions. Examples of the latter (with year of occurrence and rough location) include Northridge (1994, 34.3°N, 118.6°W), Landers (1992, 34.2°N, 116.4°W), Oceanside (1986, 33°N, 117.8°W), Elmore Ranch/Superstition Hills (1987, 33°N, 115.8°W), and Coalinga (1983, 36.3°N, 120.2°W). Large areas of ongoing seismicity include the San Jacinto Fault Zone (running NW from about 33.2°N, 116°W) and the southern Sierra Nevada and Tehachapis (34.8° − 36°N, 119.2° − 118°W) (see Figure 7 for locations of faults and geographical features mentioned in text). Note the large amount of scatter in the locations of the Coalinga events. This scatter is due to the fact that the locations of events that are outside the SCSN network (mostly Coalinga and offshore events) are subject to much larger errors than those events within the network. Depths are particularly unreliable in these regions, and sometimes the location depths cluster at both the top and the bottom of the model.

6.2. Event Depths

In most cases, accurately resolving depth is the most challenging part of earthquake location. This results from the fact that recording stations are confined to the Earth's surface, stations are often not available immediately above the events, and there is typically a strong trade-off between event depth and origin time. Finally, the true depth of earthquakes is very hard to determine independently, preventing any direct test of the accuracy of computed earthquake depths. As we mentioned in the introduction and will discuss further below, tests are possible in the case of surface explosions, but these provide only limited constraints on the locations of deeper events in the same region.

Although it is hard to access the accuracy of an individual earthquake depth estimate, some indication of the reliability of an earthquake location method may be obtained by studying the overall distribution of depths in an event catalog. In Figure 8 we plot histograms of the event depths for our final SSST locations.

Although the true distribution of event depths in southern California is unknown, we can make some judgments based on the following criteria: (1) Natural seismicity should taper to zero at zero depth since earthquake hypocenters are rarely, if ever, at the surface, (2) artificial events should cluster near zero depth, and (3) over a large heterogeneous region, such as southern California, seismicity histograms should exhibit smooth changes with depth, without sharp peaks or changes at specific depths. Figure 8a shows our entire catalog which contains a mixture of natural and artificial events. However, following *Agnew* [1990], we can largely isolate the natural seismicity by considering only nighttime events. Figure 8b plots 150,743 events from our catalog between 1900 and 0700 PST. Finally, considering that natural seismicity occurs with equal probability at any time of day, the artificial events may be isolated

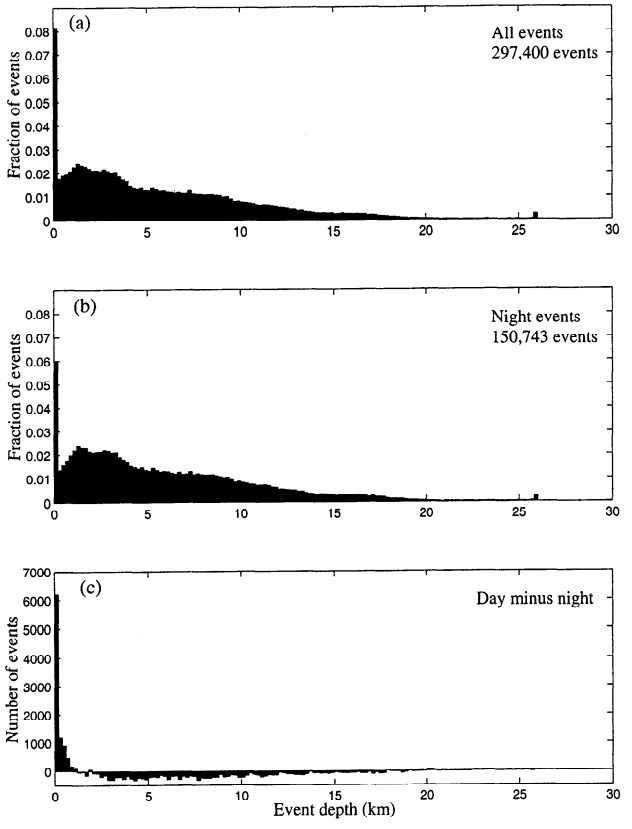

Figure 8. Histograms of the depth distribution of our source-specific station term relocations. (a) All events, which should be a mixture of natural seismicity and blasts. (b) Only those events taking place during nighttime hours (1900 to 0700 PST) and so should include almost exclusively natural seismicity. (c) Difference of the histograms of the depths of day and night events, as an approximation to the depth distribution of artificial seismicity. As expected, this histogram is strongly peaked near the surface.

by subtracting the nighttime event histogram from the daytime histogram. This difference is plotted in Figure 8c.

Approximately 6% of the natural events in Figure 8b are at the surface. This concentration results from the cutoff in the model at zero depth; these events in a sense would be better located above the surface. The number of events in the spike could be accommodated in an additional 900-m-thick layer just above the surface, assuming the event density just below the surface is representative of the events in this spike. The median standard error of our locations is 741 m; thus at least some of the spike would result from random scatter in the locations if the seismicity extends to the surface. However, this is unlikely as it is generally believed that there are few earthquakes within the top 1 or 2 km of the crust. Thus the fraction of events indicated by Figure 8b to be within the top 3 km of crust is probably unrealistically high.

The approximation to a histogram of the cultural events provided by Figure 8c is also of interest. The slight negative values at depth result from the fact that there are slightly more deep events at night than during the daytime hours, perhaps as a result of quieter conditions during the night so that more events can be detected. Most of the events occur very near zero depth, as would be expected for quarry blasts or other artificial explosions.

These results suggest that some improvement to our locations might be achieved by increasing the depths of the most shallow events. It is possible that could be done by assuming slower seismic velocities in the near surface than our current model, and this will be a topic of future research.

6.3. Other Models

The SCSN produces a catalog of events that provides a standard set of locations and magnitudes for all recorded events in southern California. However, it has long been recognized that the accuracy of these locations could be improved, and a number of researchers

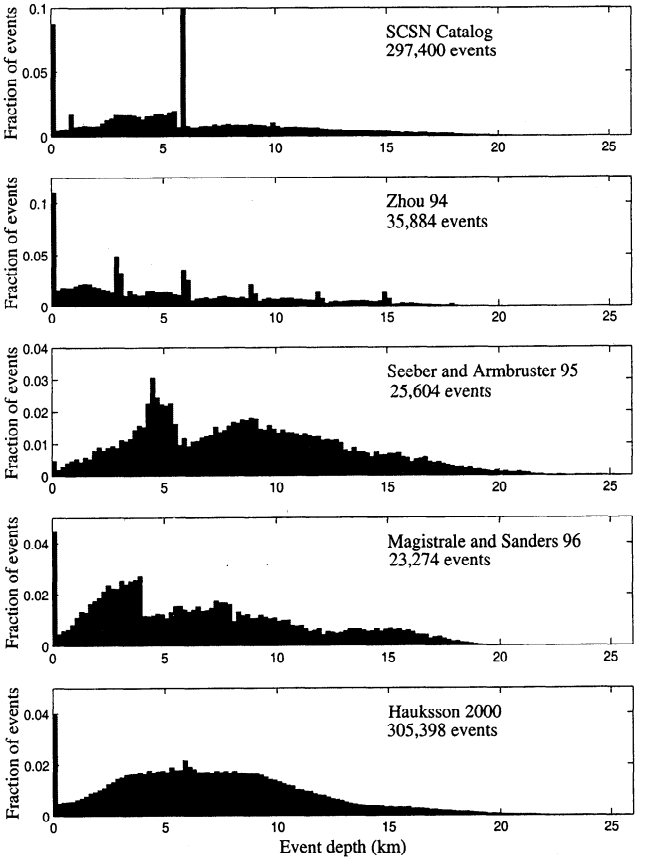

Figure 9. Histograms of the depth distributions of several other catalogs of southern California seismicity. The plot of the SCSN catalog has been clipped at 10%; in actuality, ~18% of the catalog depths fall in the bin at 6 km.

have produced revised locations for many of these events. These include the following:

1. *Zhou* [1994] performed a joint-hypocenter-velocity (JHV) inversion. *Magistrale and Zhou* [1996] selected 35,884 of these events in a study of maximum earthquake depth in southern California.

2. *Seeber and Armbruster* [1995] used a number of different regional one-dimensional velocity models, calibration events, and station terms within 8 km by 8 km boxes to produce a catalog of 7000 events in the vicinity of the Transverse Ranges. They recently updated their results to 25,604 events (J. G. Armbruster, personal communication, 1999); we obtained their current catalog from the SCEC Data Center.

3. *Magistrale and Sanders* [1996] performed a joint-hypocenter-velocity (JHV) inversion to relocate 23,274 events in the San Gorgonio Pass region.

4. *Hauksson* [2000] located 305,398 events using a three-dimensional velocity model based on a joint-hypocenter-velocity (JHV) inversion.

Depth histograms for these models, together with the SCSN catalog are plotted in Figure 9. Clearly there are large differences in the depth distribution of events in these catalogs. Some of this might result from regional differences in coverage, but there are also obvious artifacts in several of the histograms. The SCSN catalog has a large spike at 6 km depth that contains 18% of the events in the catalog; this results directly from the location algorithm in which poorly constrained locations are assigned a fixed depth of 6 km. The sharp changes seen in some of the other histograms suggests that locations may have a tendency to stick at particular depths. The *Hauksson* [2000] catalog is a notable exception, having a relatively smooth depth distribution.

It is not our purpose here to systematically compare all of these models (they were computed for different purposes using a variety of different assumptions) but to use them to test and evaluate the effectiveness of our location method. Accordingly, we have compared our results in detail with these catalogs for a number of different regions and seismicity clusters. Comparison between different catalogs is necessarily somewhat subjective because the true earthquake locations are unknown. We have concluded, however, that our results in most regions are comparable to those obtained previously using joint-hypocenter-velocity inversions. In fact, in many cases our locations exhibit greater clustering into coherent features, such as alignment into linear and planar structures, than is seen in the JHV locations. This suggests that our locations are more accurate in these cases because there is nothing intrinsic to our algorithm that should cause randomly scattered events to cluster into coherent features.

We caution, however, that this assessment applies largely to the relative locations between adjacent events, not the absolute locations of event clusters. In principle, absolute locations should be better resolved with JHV inversions (or custom one-dimensional models) than with our approach, but this is difficult to independently assess.

6.4. Close-ups and Cross Sections

The differences between the catalog locations and our relocations are most evident in close-ups of specific clusters of events. Here we select a few examples for detailed comparisons.

6.4.1. Garlock fault. Events on and near the Garlock fault just south of the El Paso Mountains are plotted in Plate 2, both in map view and a SSE-NNW cross section across part of the Garlock fault. Plate 2 (top) shows the SCSN catalog locations, Plate 2 (middle) shows our locations obtained with static station terms only, and Plate 2 (bottom) plots our final locations computed using source-specific station terms. The largest cluster of events south of the Garlock fault consists of explosions associated with mining activity in this area (see Plate 4). As measured by the degree of clustering and alignment of the seismicity into linear features, our locations, particularly the SSST locations, are significantly improved compared to the SCSN catalog. Note the separation of the cluster just SE of the Garlock fault into two tighter, temporally associated clusters. Most earthquakes near the Garlock fault are offset to the north of the surface expression of the fault, but a separate cluster of a few events occurs more directly under the fault trace. These results hint at fault complexity in this region and a possible double seismic zone. Our locations in this region are in general agreement with the JHV inversion results of *Zhou* [1994], *Seeber and Armbruster* [1995], and *Hauksson* [2000], although only the Hauksson catalog has a comparable number of events.

6.4.2. Rose Canyon fault zone. A comparison of locations for events near San Diego, California, including a cross section of 1985–1987 swarms of seismicity in the Rose Canyon fault zone is shown in Plate 3. Again, our locations show considerable improvement over the SCSN catalog. The improvement achieved with the source-specific station terms is more dramatic in this case than the Garlock example, perhaps because the static station terms are poorly suited to this region (located at the edge of the SCSN network). Our final locations for the Rose Canyon cluster show scatter comparable to that obtained by *Magistrale* [1993] with a custom velocity model.

6.4.3. Whittier Narrows aftershocks. The 1987 Whittier Narrows earthquake ($M = 6.0$) occurred on a shallow dipping blind-thrust fault at ~10 to 15 km depth in the northern part of the Los Angeles Basin, just south of Pasadena, California. Figure 10 compares S-N cross sections of the catalog locations, our static station term locations, and our SSST locations. The blurring effect of scatter in event depths is particularly dramatic in this example owing to

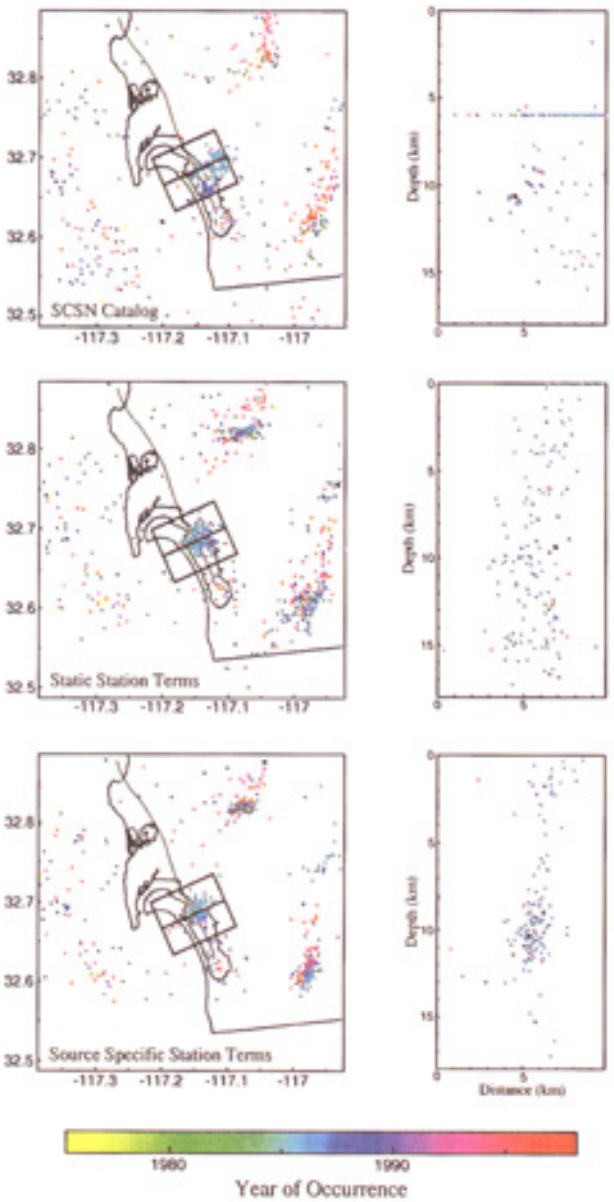

Plate 3. (left) Map views and (right) WSW-ENE cross sections of (top) the SCSN catalog locations, (middle) our static station term relocations, and (bottom) our source-specific station term relocations of seismicity in southwestern San Diego County.

the nearly horizontal distribution of the aftershocks. Our results here are comparable in relative location accuracy to those obtained by *Shearer* [1997] using a custom set of station terms specific to these events. The absolute depths of the aftershocks agree with the revised Whittier Narrows depths computed by *Shaw and Shearer* [1999] in which the shallow velocity structure of nearby stations was calibrated using borehole velocity logs. For comparison, JHV locations for these events [e.g., *Zhou*, 1994; *Seeber and Armbruster*, 1995; *Hauksson*, 2000] show improvement compared to the SCSN catalog but have considerably more scatter than our results.

6.5. Natural Versus Anthropogenic Seismicity

Many of these events are quarry or construction blasts rather than natural seismicity. As pointed out by *Agnew* [1990], the distribution of the time of day of occur-

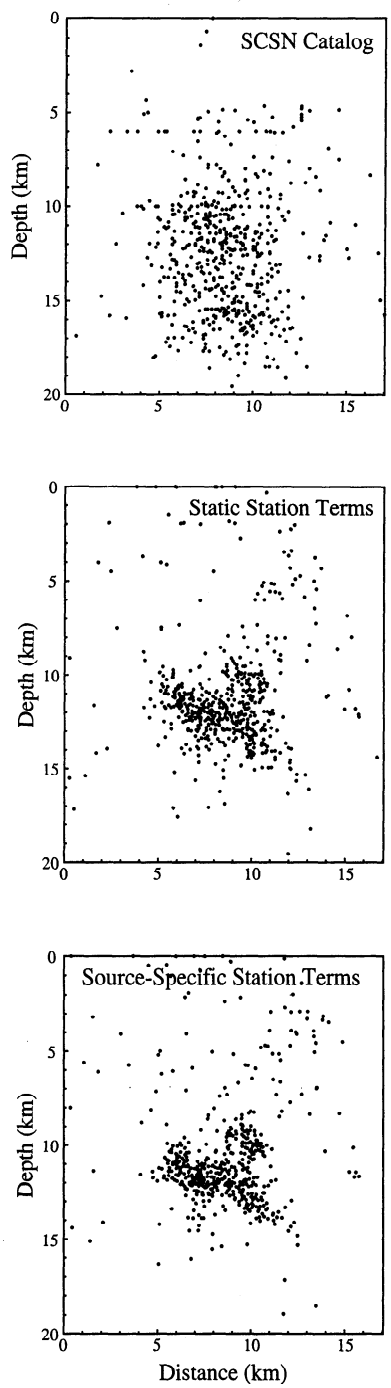

Figure 10. S-N cross sections of the Whittier Narrows earthquake and its aftershocks, (top) SCSN catalog locations, (middle) our static station term relocations, and (bottom) our final source specific station term relocations. The cross sections are centered at 34.055°N, 118.085°W.

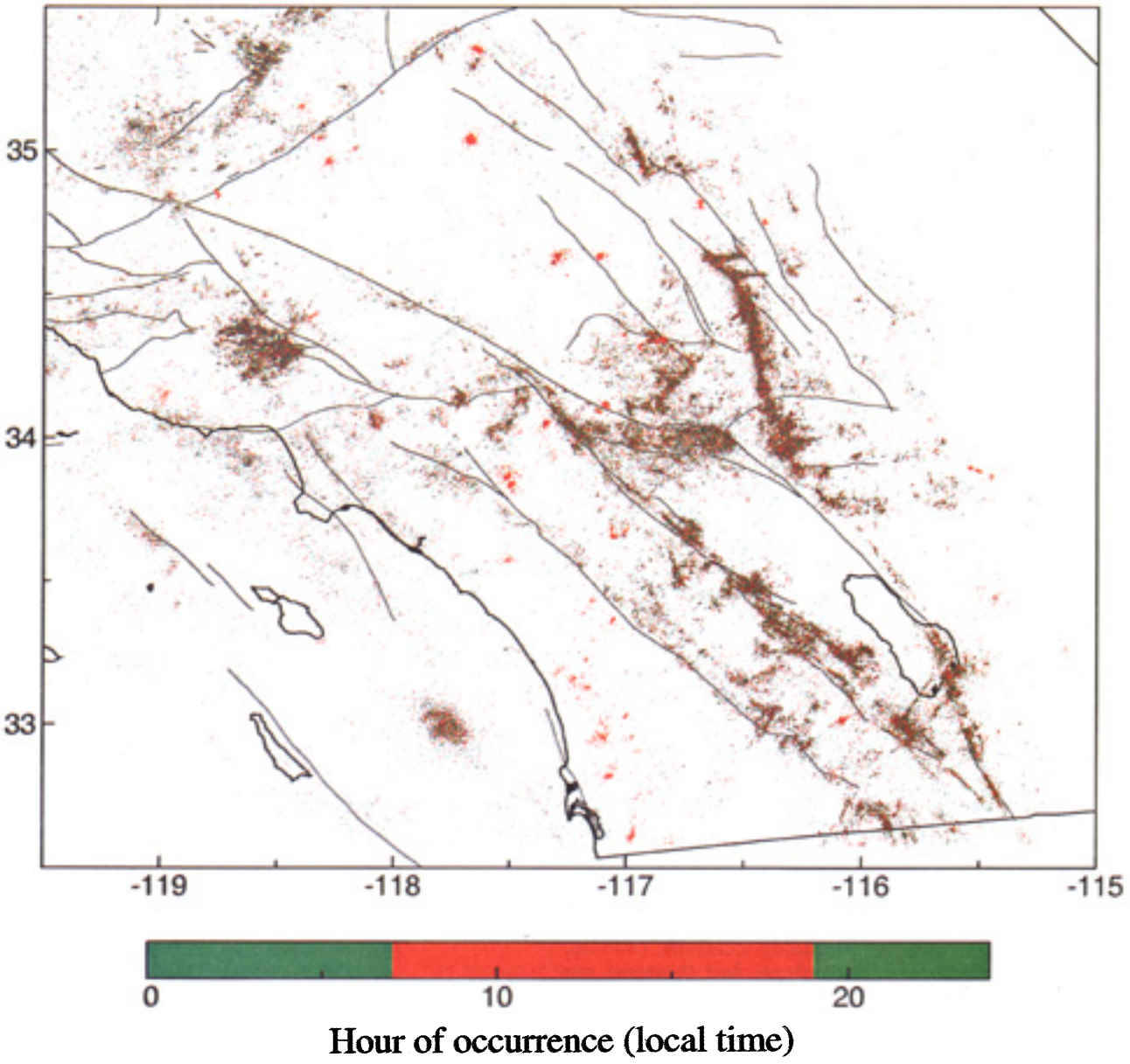

Plate 4. Map view of our final relocations with the events colored red or green according to whether they occurred during the day (0700 to 1900 PST) or the night, respectively. Since virtually all quarry and construction blasts take place during the day (while natural seismicity occurs at all hours), areas of natural seismicity appear mottled red and green, while quarries and construction areas appear as coherent red clusters.

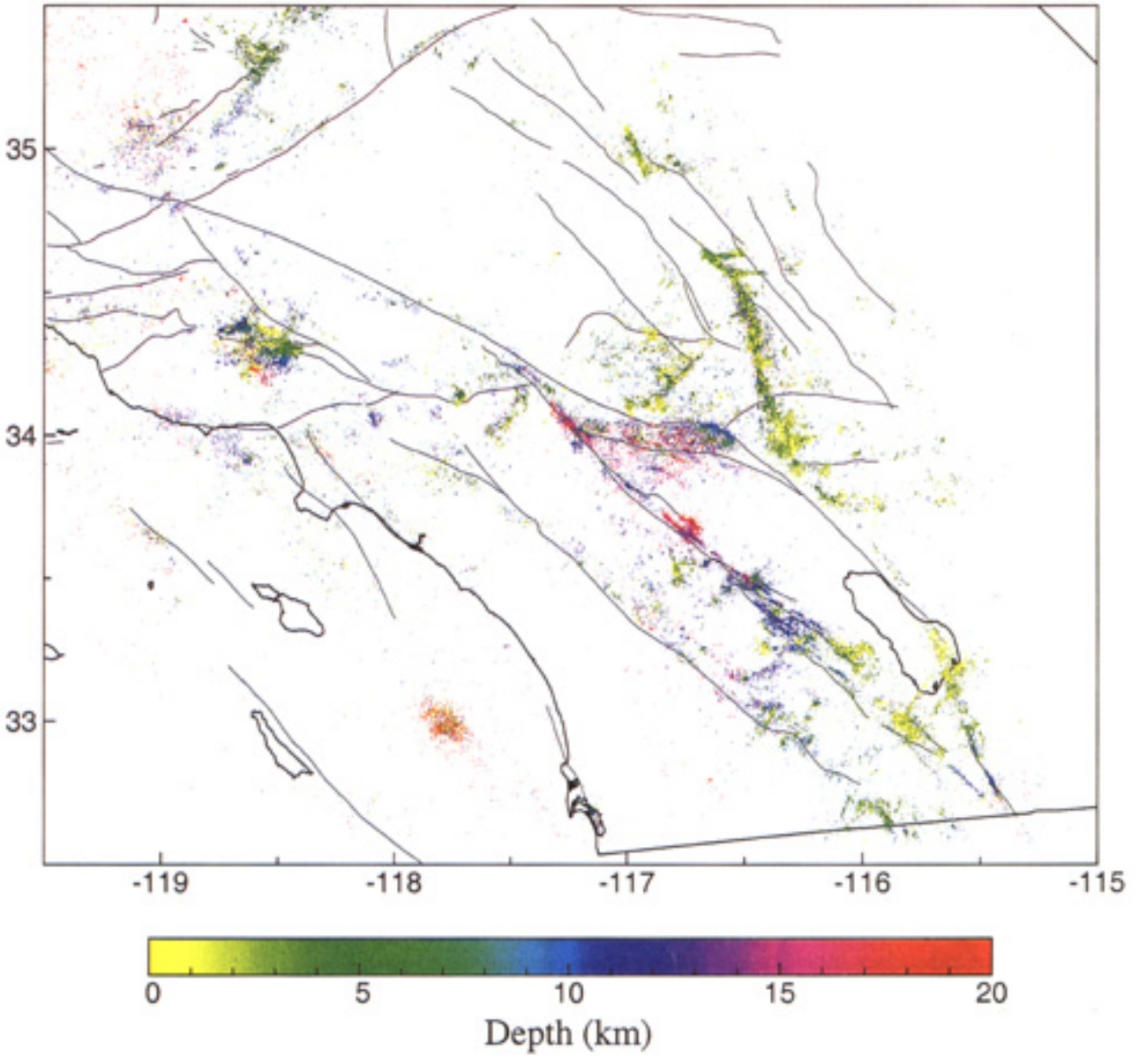

Plate 5. Map view of our final relocations of the events which occurred at night, with the events colored according to their depth. This plot should contain almost exclusively natural seismicity. Vertical and steeply dipping faults appear as a mixture of the colors appropriate to the range of depths over which they are seismically active. The color of shallowly dipping faults changes in the direction of dip, the most obvious example in this plot is Northridge which dips roughly south and thus changes from red, through blue and green, to yellow from south to north.

rence of events within a cluster can help to discriminate between natural and cultural activity. That is, natural seismicity occurs with equal probability at all times during the day, while almost all quarry and construction blasts are set off during daylight/working hours. Plate 4 plots all events with those occurring during the daytime (0700 to 1900 hours PST) in red and the nighttime events in green. Natural seismicity appears as areas of mixed red and green, while quarries and areas of construction blasts appear as coherent red blobs. It is clear from this plot that most of the clusters within the Mojave block, north of the San Andreas Fault and south of the Garlock fault are artificial. Similarly, most of San Diego County west of the Elsinore Fault is aseismic (with the exception of the Rose Canyon fault zone, see section 6.4).

A notable exception to the rule that all cultural events occur during the daytime is provided by the line of nighttime events near 34.3°N, 117.85°W. This is one of the Los Angeles Region Seismic Experiment (LARSE) [*Fuis et al.*, 1995] shot lines, which was set off at night to take advantage of the lower cultural noise levels at night at stations in the Los Angeles Basin. To give a more accurate impression of the natural seismicity, Plate 5 plots just the nighttime events. This should include roughly half of the natural seismicity but almost none of the explosions. In Plate 5 the events are colored by their depth rather than their date of occurrence. Thus vertical and steeply dipping faults appear as a mixture of the colors appropriate to the range of depths over which they are seismically active. Shallowly dipping faults change color in the direction of dip; the most obvious example in this plot is the Northridge aftershock sequence, which dips roughly south and thus changes from red, through blue and green, to yellow from south to north.

6.6. Maximum Depth of Seismicity

The depth extent of seismicity in a given region provides limits on the brittle-ductile transition depth and clues about the subsurface lithology and temperatures [e.g., *Magistrale and Zhou*, 1996]. Plate 6 plots a measure of the maximum depth extent of the seismicity in our relocated catalog across southern California. To produce this plot, we divide southern California into 5 km × 5 km bins and find the 90th percentile depth of all events in each bin (excluding those events which are "stuck" to the surface or to the bottom of the velocity model). These depths are then smoothed with a 3 × 3 median filter. Finally, we color each bin by depth according to the colorscale. We exclude events outside the network from this plot owing to the unreliability of their depths.

Deep areas of seismicity are noteworthy in several regions. A large deep region (near -116.9°, 33.9°) is imaged along and north of the San Jacinto fault near San Jacinto peak. The San Andreas fault appears to

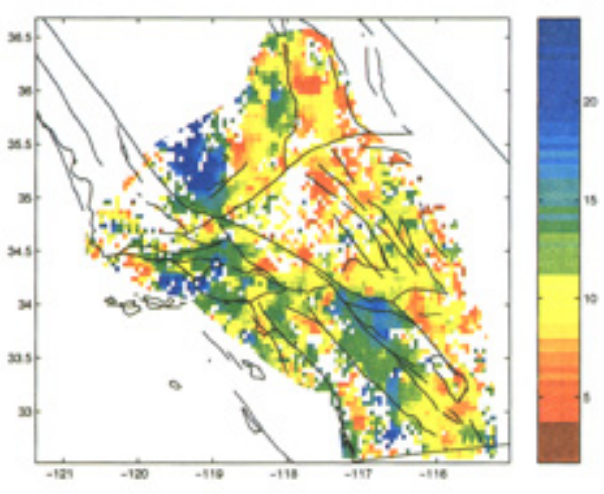

Plate 6. Maximum depth of seismicity (in km) as approximated by the 90th percentile of event depths in 5 km × 5 km boxes; see text for details.

mark the northern edge of this deep region, as noted by *Magistrale and Zhou* [1996]. The southern boundary of this deep region is less clear but appears in some areas to extend south of the Elsinore fault. Another zone of deep seismicity (near -119.3°, 34.2°) is seen in the Ventura Basin, agreeing with previous observations of deep events in this area by *Bryant and Jones* [1992]. Anomalously low heat flow has been observed in the Ventura Basin [*De Rito et al.*, 1989], and the tomographic images of *Humphreys and Clayton* [1990] show higher than average P velocities, suggesting that colder temperatures and brittle behavior extend to greater depths in this region. Another large deep region (near -119.2°, 35.2°) is seen in the southern end of the Central Valley. Depths for the Central Valley events are of questionable accuracy but the southernmost part of this region (near Mount Piños) appears to be well resolved.

7. Discussion

Earthquake locations are one of the primary products of modern seismological research and provide invaluable information on the locations of subsurface faults. It is not surprising, therefore, that considerable effort has gone into improving the accuracy of earthquake locations. Most of the ideas that we have implemented in our relocation approach (the L1 norm, grid search, spatially varying station terms) have been previously described by other authors. The most original part of our method is the use of natural neighbor smoothing to compute source-specific station terms. This technique is a key part of our overall goal: to develop a practical method for relocating large, distributed areas of seismicity that achieves the greatest possible relative location accuracy within local clusters of events.

Locations in any large earthquake catalog are almost certainly never as accurate as could be achieved by de-

tailed analysis of a particular region. Indeed, many parts of the SCSN catalog have been the subject of more detailed investigations which have involved use of custom velocity models specific to a particular region. Other studies have used subsets of the events in simultaneous inversions for locations and three-dimensional velocity structure. None of these studies, however, have relocated more than a fraction of the total events in the SCSN catalog. For this reason, the SCSN catalog remains an important source of information for earthquake locations in southern California.

Many of the sophisticated relocation methods that have been developed require considerable care in tuning of parameters to achieve optimal results, making them difficult to adapt to automatic processing for a large network. There remains a need to develop location methods that are suited to large-scale processing but achieve better results than standard catalogs. Our method requires only the P and S phase picks, the station locations, and a single one-dimensional velocity model. Because the L1 norm is robust with respect to bad picks, no editing of the data is required.

For simplicity and uniformity, we apply a single one-dimensional velocity model to relocate all of the SCSN events. In this way, we avoid edge effects between customized one-dimensional models for different regions or the complexities associated with a full three-dimensional model. By ignoring lateral velocity variations we cannot hope to achieve the absolute location accuracy that a proper three-dimensional model could provide. However, by computing source-specific station terms we can locally correct for three-dimensional structure and improve the relative location accuracy among adjacent events. In fact, our results compare quite favorably to locations obtained in several previous analyses of SCSN data using JHV inversion techniques.

Because our method is based on a grid search algorithm, it could be implemented just as efficiently for a three-dimensional velocity model, provided travel times can be computed and saved from the stations to the model grid points. Another possible future improvement would be to use shots or quarry blasts of known location as reference points, constraining the source-specific station terms at those points and thus improving the absolute location accuracy of adjacent events.

Finally, a note of caution that it is very difficult to produce a large earthquake catalog that does not have location artifacts to some degree. Some of these are easy to recognize (e.g., poorly constrained depths for events outside the network), while others are more subtle (e.g., the tendency for event clusters to divide into different groups depending upon the presence or absence of crucial picks from nearby stations). We have attempted to minimize these artifacts in our relocations, but some of them undoubtedly still remain.

Appendix A: Maximum Likelihood

In general, the observed arrival time at the jth station from the ith event will be

$$T_{ij}^{\text{obs}} = t_i + \tau_j(\vec{x_i}) + \epsilon_{ij}, \tag{A1}$$

where t_i and $\vec{x_i}$ are the origin time and location of the ith event, respectively, $\tau_j(\vec{x})$ gives the travel time to the jth station from a source at $\vec{x}$, and ϵ_{ij} is the picking error (which is modeled as the realization of a random variable). Secondary phases at the same stations can be treated as separate stations. The indices i and j run from 1 to n_q (total number of events) and n_s (total number of stations), respectively. If the joint probability density function (pdf) of the picking errors is $\phi(\epsilon_{ij})$, then the maximum likelihood estimates for the t_i and $\vec{x_i}$ are those that maximize $\phi[T_{ij}^{\text{obs}} - t_i - \tau_j(\vec{x_i})]$, or, equivalently, those that minimize the misfit function

$$C(t_i, \vec{x_i}) \equiv -\ln\left\{\phi\left[T_{ij}^{\text{obs}} - t_i - \tau_j\left(\vec{x_i}\right)\right]\right\}. \tag{A2}$$

Differentiating C with respect to each t_i and each component of each $\vec{x_i}$ would give $4n_q$ equations to solve for the $4n_q$ unknown hypocentral parameters. If the ϵ_{ij} are all independent, then the joint pdf is just the product of the individual pdf's, $\phi = \prod_{i,j} \phi_{ij}$, and the misfit function will given by

$$C(t_i, \vec{x_i}) = \sum_{i,j} \left\{-\ln \phi_{ij}\left[T_{ij}^{\text{obs}} - t_i - \tau_j(\vec{x_i})\right]\right\}. \tag{A3}$$

In this case the system of $4n_q$ equations will decouple into n_q sets of four equations, one set for each hypocenter. So each hypocentral estimate is independent of the others, and for each hypocenter we minimize the individual event misfit function

$$C_i(t_i, \vec{x_i}) \equiv \sum_{j} \left\{-\ln \phi_{ij}\left[T_{ij}^{\text{obs}} - t_i - \tau_j(\vec{x_i})\right]\right\}. \tag{A4}$$

For example, if $\phi_{ij} \propto \exp\left(-k\left|\epsilon_{ij}/\sigma_{ij}\right|^p\right)$ (if $p = 2$ or $p = 1$, then ϵ_{ij} are zero-mean Gaussian or double-sided exponential random variables, respectively), then the overall misfit function will be given by

$$C(t_i, \vec{x_i}) = \sum_{i,j} w_{ij}\left|T_{ij}^{\text{obs}} - t_i - \tau_j(\vec{x_i})\right|^p, \tag{A5}$$

and the individual event misfit functions by

$$C_i(t_i, \vec{x_i}) = \sum_{j} w_{ij}\left|T_{ij}^{\text{obs}} - t_i - \tau_j(\vec{x_i})\right|^p, \tag{A6}$$

with $w_{ij} \equiv 1/{\sigma_{ij}}^p$. Note that we dropped the common factor k since it will not affect the minimization. Also, the sums run over only those values of i and j for which a T_{ij}^{obs} exists, or, alternatively, i can take on all values

between 1 and n_q and j all values from 1 to n_s if w_{ij} is set to zero if no T_{ij}^{obs} exists.

The weights w_{ij} should be determined from an estimate of the spread of the random picking error distribution and will vary from pick to pick (depending on the signal-to-noise ratio of the arrival). Unfortunately, analyst estimates of the picking error are only available for approximately half of the events in the SCSN catalog. In experiments using our procedure on subsets of that part of the SCSN catalog for which such estimates are available, we found that the locations determined using weights based on picking error estimates were not very different from those found with all weights set to 1.0. Thus, in order to use more of the SCSN catalog we use a weight of 1.0 for all picks. This also speeds the procedure somewhat since the median is faster to compute than the weighted median (used to calculate the origin times and station corrections; see text and Appendix B).

Appendix B: Weighted median

The weighted median is a generalization of the usual median. The usual median solves the problem: for a given set of numbers z_j, find the μ which minimizes the function $f(\mu) = \sum_j |z_j - \mu|$. This function is continuous, but piecewise linear, with discontinuities in its slope at each of the z_j. Such a function's extrema will occur where the derivative is zero or where the derivative discontinuously changes sign. The derivative with respect to μ is $f'(\mu) = \sum_j \text{sgn}(\mu - z_j)$, where $\text{sgn}(x)$ is defined to be -1 if $x < 0$ and $+1$ if $x > 0$ (and is undefined if $x = 0$). Thus the derivative is simply given by the difference between the number of z_j which are less than μ and the number of z_j which are greater than μ. If there are an even number of z_j and the two middle z_j (when the z_j are sorted into ascending order) are distinct, any value of μ between the two middle z_j will have the derivative equal to zero and the same minimum value of $f(\mu)$. The convention in this case is to take the median to be the mean of the two middle z_j. If there are an odd number of z_j (or the middle two of an even number of z_j are not distinct), the derivative will discontinuously change sign when μ is equal to the middle z_j (or the common value of the middle two z_j) and so $f(\mu)$ will have a unique minimum there.

The weighted median solves the following generalization of the above problem: Given a set of numbers z_j and associated positive weights w_j, find the μ that minimizes $g(\mu) = \sum_j w_j |z_j - \mu|$. The comments above on the continuity of f and its derivative and the location of the extrema of f also apply to g and its derivative. The derivative with respect to μ is $g'(\mu) = \sum_j w_j \text{sgn}(\mu - z_j)$. In this case the derivative is given by the difference between the sum of the weights associated with the z_j which are less than μ and that of those associated with the z_j which are greater than μ. Again there will either be an interval in which any value of μ has the derivative equal to zero and the same minimum value of g (in which case we will take the weighted median to be the midpoint of that interval) or there will be a unique value of μ at which the derivative discontinuously changes sign and where g takes on its unique minimum value. So to find the weighted median, (1) sum the weights w_j and denote the sum by W; (2) sort the z_j (and associated w_j) in order of ascending z_j; (3) form partial sums $\sum^{j_0} w_j$ to find the smallest value of j_0 for which the partial sum equals or exceeds $W/2$. If the partial sum in step (3) exactly equals $W/2$, the weighted median is defined to be the mean of z_{j_0} and z_{j_0+1}, otherwise, it is z_{j_0}.

Appendix C: Full Algorithm

To avoid some artifacts in areas of southern California in which our 1-D velocity model is particularly inappropriate, we first work with only those events which have at least one S pick within 25 km of the epicenter (in the rest of this appendix we will refer to these events as the S events and the other events as the non-S events). The S events make up approximately two thirds of the catalog. We then add in the non-S events later, initially, using the SSSTs determined from the S events.

1. First, locate the S events using steps 1-5 of the basic algorithm.

2. Next, locate the non-S events using the static station terms of Figure 3.

3. Construct the 2-D Delaunay tessellation of the locations of all events, using the locations from step C1 for the S events and the locations from step C2 for the non-S events. We use a 2-D tessellation in this step because we do not trust the depths of the non-S events from the previous step.

4. Calculate SSSTs for the non-S events from the residuals of the nearest natural neighbor S events. As in step 3, we don't yet trust the depths of the non-S events, so we use only the residuals from the S events in calculating the SSSTs.

5. Locate the non-S events using the SSSTs from the previous step.

6. Construct the 3-D Delaunay tessellation of the locations of all events, using the locations from step C1 for the S events and the locations from step 5 for the non-S events.

7. Calculate SSSTs for the non-S events from the residuals of the nearest natural neighbor S events.

8. Relocate the non-S events using the SSSTs from step 7.

9. Finally, combine the events and iterate steps 2, 3, and 4 of the basic algorithm (with all events) to convergence.

Acknowledgments. We are grateful to the operators and analysts who maintain the USGS/Caltech Southern California Seismic Network and who pick and archive the seismograms and to the personnel at the Southern California Earthquake Center who distribute the data. We also thank

Clifford Thurber, Lee Steck, and Cliff Frohlich for reviews which improved this manuscript. We thank Egill Hauksson for providing us with the shot locations used in section 5.7. This work was supported by the Southern California Earthquake Center. SCEC is funded by NSF Cooperative Agreement EAR-8920136 and USGS Cooperative Agreements 14-08-001-A0899 and 1434-HQ-97AG01718. This research was also funded by NEHRP/USGS grants 1434-94-G-2454 and 1434-HQ-97-GR-03162.

References

Agnew, D., The use of time-of-day seismicity maps for earthquake/explosion discrimination by local networks, with an application to the seismicity of San Diego county, *Bull. Seismol. Soc. Am.*, *80*, 747–750, 1990.

Anderson, K., Robust earthquake location using M-estimates, *Phys. Earth Planet. Inter.*, *30*, 119–130, 1982.

Barber, C., D. Dobkin, and H. Huhdanpaa, The quickhull algorithm for convex hulls, *Trans. Math. Software*, *22*, 469–483, 1996.

Billings, S., M. Sambridge, and B. Kennett, Errors in hypocenter location: Picking, model, and magnitude dependence, *Bull. Seismol. Soc. Am.*, *84*, 1978–1990, 1994.

Braun, J., and M. Sambridge, A numberical method for solving partial differential equations on highly irregular evolving grids, *Nature*, *376*, 655–660, 1995.

Bryant, A., and L. Jones, Anomalously deep crustal earthquake in the Ventura Basin, southern California, *J. Geophys. Res.*, *97*, 437–447, 1992.

Buland, R., Residual statistics, *Terra Cognita*, *4*, 268, 1984.

Cleary, J., and A. Hales, An analysis of the travel times of P waves to north american stations in the distance range 30° to 100°, *Bull. Seismol. Soc. Am.*, *56*, 467–489, 1966.

Cogbill, A., and L. Steck, Use of propagation path corrections to improve regional event locations in western China, *Eos Trans. AGU*, *78*(46), Fall Meet. Suppl., F445, 1997.

Constable, C., R. Parker, and P. Stark, Geomagnetic field models incorporating frozen-flux constraints, *Geophys. J. Int.*, *113*, 419–433, 1993.

De Rito, R., A. Lachenbruch, T. Moses, and R. Munroe, Heat flow and thermotectonic problems of the central Ventura Basin, southern california, *J. Geophys. Res.*, *94*, 681–699, 1989.

Douglas, A., Joint epicentre determination, *Nature*, *215*, 47–48, 1967.

Dziewonski, A., and D. Anderson, Travel times and station corrections for P waves at teleseismic distances, *J. Geophys. Res.*, *88*, 3295–3314, 1983.

Eberhart Phillips, D., Three-dimensional P and S velocity structure in the Coalinga region, California, *J. Geophys. Res.*, *95*, 15,343–15,363, 1990.

Eberhart Phillips, D., and A. Michael, Three-dimensional velocity structure, seismicity, and fault structure in the Parkfield region, central California, *J. Geophys. Res.*, *98*, 15,737–15,758, 1993.

Evernden, J., Precision of epicentres obtained by small numbers of world-wide stations, *Bull. Seismol. Soc. Am.*, *59*, 1365–1398, 1969.

Freedman, H., The 'little variable factor': A statistical discussion of the reading of seismograms, *Bull. Seismol. Soc. Am.*, *56*, 593–604, 1966.

Frohlich, C., An efficient method for the joint hypocenter determination for large groups of earthquakes, *Comput. Geosci.*, *5*, 387–389, 1979.

Fuis, G., T. Brocher, K. Klitgord, D. Okaya, T. Henyey, R. Clayton, T. Ryberg, and W. Lutter, An overview of preliminary seismic images from the Los Angeles Region Seismic Experiment (LARSE), *Eos Trans. AGU*, *76*(46), Fall Meet. Supl., F347, 1995.

Geiger, L., Herdbestimmung bei Erdbeben aus den Ankunftszeiten, *Nachr. Ges. Wiss. Göttingen Math. Phys. Kl.*, *4*, 331–349, 1910.

Hadley, D., and H. Kanamori, Seismic structure of the Transverse Ranges, California, *Geol. Soc. Am. Bull.*, *88*, 1469–1478, 1977.

Hauksson, E., Crustal structure and seismicity distribution adjacent to the Pacific and North America plate boundary in southern California, *J. Geophys. Res., in press*, 2000.

Hawley, B., G. Zandt, and R. Smith, Simultaneous inversion for hypocenters and lateral velocity variations: An iterative solution with a layered model, *J. Geophys. Res.*, *86*, 7073–7086, 1981.

Herrin, E., and J. Taggart, Regional variations in P travel times, *Bull. Seismol. Soc. Am.*, *58*, 1325–1337, 1968.

Hildebrand, J., and R. Parker, Paleomagnetism of Cretaceous Pacific seamounts revisited, *J. Geophys. Res.*, *92*, 12,695–12,712, 1987.

Huber, P., *Robust Statistics*, John Wiley, New York, 1981.

Humphreys, E., and R. Clayton, Tomographic image of the southern California mantle, *J. Geophys. Res.*, *95*, 19,725–19,746, 1990.

Jeffreys, H., An alternative to the rejection of observations, *Proc. R. Soc. London, Ser. A*, *137*, 78–87, 1932.

Jordan, T., and K. Sverdrup, Teleseismic location techniques and their application to earthquake clusters in the south-central Pacific, *Bull. Seismol. Soc. Am.*, *71*, 1105–1130, 1981.

Kendall, M., and A. Stuart, *The Advanced Theory of Statistics, vol. 2, Inference and Relationship*, Hafner, New York, 1967.

Lilwall, R., and A. Douglas, Estimation of P-wave travel times using the joint epicentre method, *Geophys. J. R. Astron. Soc.*, *19*, 165–181, 1970.

Magistrale, H., Seismicity of the Rose Canyon fault zone near San Diego, California, *Bull. Seismol. Soc. Am.*, *83*, 1971–1978, 1993.

Magistrale, H., and C. Sanders, Evidence from precise earthquake hypocenters for segmentation of the San Andreas fault in San Gorgonio pass, *J. Geophys. Res.*, *101*, 3031–3044, 1996.

Magistrale, H., and H. Zhou, Lithologic control of the depth of earthquakes in southern California, *Science*, *273*, 639–642, 1996.

Michael, A., Effects of three-dimensional velocity structure on the seismicity of the 1984 Morgan Hill, California, aftershock sequence, *Bull. Seismol. Soc. Am.*, *78*, 1199–1221, 1988.

Minster, J.-B., N. Williams, T. Masters, J. Gilbert, and J. Haase, Application of evolutionary programming to earthquake hypocenter determination, in *Evolutionary Programming; Proceedings of the Fourth Annual Conference on EP*, edited by J. McDonnell, pp. 3–17, MIT, Cambridge, 1995.

Nelson, G., and J. Vidale, Earthquake locations by 3-D finite-difference travel times, *Bull. Seismol. Soc. Am.*, *80*, 395–410, 1990.

Parker, R., L. Shure, and J. Hildebrand, The application of inverse theory to seamount magnetism, *Rev. Geophys.*, *25*, 17–40, 1987.

Pavlis, G., and J. Booker, The mixed discrete-continuous inverse problem; application to the simultaneous determination of earthquake hypocenters and velocity structure, *J. Geophys. Res.*, *85*, 4801–4810, 1980.

Pavlis, G., and J. Booker, Progressive multiple event location (PMEL), *Bull. Seismol. Soc. Am.*, *73*, 1753–1777, 1983.

Pavlis, G., and N. Hokanson, Separated earthquake location, *J. Geophys. Res.*, *90*, 12 777–12,789, 1985.

Pujol, J., Comments on the joint determination of hypocenters and station corrections, *Bull. Seismol. Soc. Am.*, *78*, 1179–1189, 1988.

Pulliam, R., D. Vasco, and L. Johnson, Tomographic inversion for mantle P wave velocity structure based on the minimization of l^2 and l^1 norms of International Seismological Centre travel time residuals, *J. Geophys. Res.*, *98*, 699–734, 1993.

Robertson, G., and J. Woodhouse, Comparison of P and S station corrections and their relationship to upper mantle structure, *J. Geophys. Res.*, *102*, 27,355–27,366, 1997.

Sambridge, M., and K. Gallagher, Earthquake hypocenter location using genetic algorithms, *Bull. Seismol. Soc. Am.*, *83*, 1467–1491, 1993.

Sambridge, M., and B. Kennett, A novel method of hypocentre location, *Geophys. J. R. Astron. Soc.*, *87*, 679–697, 1986.

Sambridge, M., J. Braun, and H. McQueen, Geophysical parameterization and interpolation of irregular data using natural neighbours, *Geophys. J. Int.*, *122*, 837–857, 1995.

Schultz, C., S. Myers, J. Hipp, and C. Young, Nonstationary bayesian kriging: A predictive technique to generate spatial corrections for seismic detection, location, and identification, *Bull. Seismol. Soc. Am.*, *88*, 1275–1288, 1998.

Seeber, L., and J. Armbruster, The San Andreas fault system through the Transverse Ranges as illuminated by earthquakes, *J. Geophys. Res.*, *100*, 8285–8310, 1995.

Shaw, J., and P. Shearer, An elusive blind-thrust fault beneath metropolitan Los Angeles, *Science*, *283*, 1516–1518, 1999.

Shearer, P., Improving local earthquake locations using the L1 norm and waveform cross correlation: Application to the Whittier Narrows, California, aftershock sequence, *J. Geophys. Res.*, *102*, 8269–8283, 1997.

Smith, E., An efficient algorithm for routine joint hypocentre determination, *Phys. Earth Planet. Inter.*, *30*, 135–144, 1982.

Spencer, C., and D. Gubbins, Travel-time inversion for simultaneous earthquake location and velocity structure determination in laterally varying media, *Geophys. J. R. Astron. Soc.*, *63*, 95–116, 1980.

Thurber, C., Earthquake locations and three-dimensional crustal structure in the Coyote Lake area, central California, *J. Geophys. Res.*, *88*, 8226–8236, 1983.

Thurber, C., Analysis methods for kinematic data from local earthquakes, *Rev. Geophys.*, *24*, 793–805, 1986.

Viret, M., G. Bollinger, J. Snoke, and J. Dewey, Joint hypocenter relocation studies with sparse data sets—A case history: Virginia earthquakes, *Bull. Seismol. Soc. Am.*, *74*, 2297–2311, 1984.

Wald, L., L. Hutton, and D. Given, The Southern California Network Bulletin: 1990-1993 summary, *Seismol. Res. Lett.*, *66*, 9–19, 1995.

Zhou, H.-W., Crustal P and S velocities in southern California from a master station inversion using fresnel volume rays, *Eos Trans. AGU*, *75*(44), Fall Meet. Suppl., F483–F484, 1994.

Zhou, H.-W., and H. Wang, A revisit to P wave travel time statics at teleseismic stations, *J. Geophys. Res.*, *99*, 17,849–17,862, 1994.

K. B. Richards-Dinger and P. M. Shearer, Institute of Geophysics and Planetary Physics, Scripps Institution of Oceanography, University of California, San Diego, La Jolla, CA 92093-0225. (kdinger@ucsd.edu)

(Received May 24, 1999; revised November 15, 1999; accepted December 20, 1999.)